Thesis for the degree of Doctor of Philosophy
in the Natural Sciences

# Micro-Crystallization and Time-Resolved Diffraction Studies of a Bacterial Photosynthetic Reaction Center

Petra Båth


UNIVERSITY OF GOTHENBURG

Department of Chemistry and Molecular Biology
Gothenburg, 2019

Thesis for the degree of Doctor of Philosophy
in the Natural Sciences

Micro-Crystallization and Time-Resolved Diffraction Studies of a Bacterial Photosynthetic Reaction Center

Petra Båth

**Cover:** A visualization of the crystal packing of a bacterial reaction center in the two crystal forms described in this thesis.

Copyright © 2019 by Petra Båth
ISBN 978-91-7833-494-0 (Print)
ISBN 978-91-7833-495-7 (PDF)
Available online at http://hdl.handle.net/2077/60187

Department of Chemistry and Molecular Biology
Division of Biochemistry and Structural Biology
University of Gothenburg
SE-405 30, Göteborg, Sweden

Printed by BrandFactory AB
Göteborg, Sweden, 2019

# Abstract

Photosynthesis is one of the most important set of chemical reactions in nature as they can convert sunlight into hydrocarbons and chemical energy. The proteins responsible for this are two general types of reaction centers that can be found in a wide variety of living organisms capable of photosynthesis, from bacteria to algae and plants. Despite the range of host cells the reaction centers themselves have fairly conserved structure and function where the absorption of light leads to an electron transfer process and eventually the production of energy. The work in this thesis is focused on the bacterial reaction center from *Blastochloris viridis*, which is an analogue to photosystem II in plants. Our studies aimed to further examine exactly what happens in the protein as light is absorbed.

X-ray crystallography has been an important tool for determining the atomic structure of proteins for several decades. This technique requires that the protein in question is in a crystalline form or else no structural data can be obtained. The development of a new generation of X-ray sources, X-ray free-electron lasers, makes new types of experiments possible but it also requires new ways of preparing crystals for the highly specialized delivery systems used. This thesis presents new ways of preparing membrane protein microcrystals for different types of delivery media. A new way to make crystals in lipidic cubic phase is presented based on setting up crystallization trials in deep-well plates and vials rather than the standard gas-tight syringes. This basic protocol has been developed to add crystal seeds as well as making crystals in an oxygen-free environment. Using this method a 2.3 Å resolution X-ray structure of reaction center was obtained from seeded crystals measuring only 20 μm. For crystals growing in vapour diffusion several techniques of generating crystals are presented depending on how far the screening protocols have been developed; initial crystals can simply be crushed into the size required and more homogeneous microcrystals can be produced by a seeding protocol. These crystals were then used in a time resolved study at an XFEL showing the structural movements of the cofactors in the protein picoseconds after photon absorption.

# Publications

This thesis consists of the following research papers:

**Paper I:** Robert Dods, **Petra Båth**, David Arnlund, Kenneth R. Beyerlein, Garrett Nelson, Mengling Liang, Rajiv Harimoorthy, Peter Berntsen, Erik Malmerberg, Linda Johansson, Rebecka Andersson, Robert Bosman, Sergio Carbajo, Elin Claesson, Chelsie E. Conrad, Peter Dahl, Greger Hammarin, Mark S. Hunter, Chufeng Li, Stella Lisova, Despina Milathianaki, Joseph Robinson, Cecilia Safari, Amit Sharma, Garth Williams, Cecilia Wickstrand, Oleksandr Yefanov, Jan Davidsson, Daniel P. DePonte, Anton Barty, Gisela Brändén, Richard Neutze.
"From macrocrystals to microcrystals: a strategy for membrane protein serial crystallography" *Structure* (2017)
doi: 10.1016/j.str.2017.07.002

**Paper II:** **Petra Båth**, Per Börjesson, Rob Bosman, Cecilia Wickstrand, Robert Dods, Tinna Björg Ulfarsdottir, Peter Dahl, María-Jose García-Bonete, Johanna-Barbara Linse, Giorgia Ortolani, Rebecka Andersson, Cecilia Safari, Elin Dunevall, Swagatha Ghosh, Eriko Nango, Rie Tanaka, Takanori Nakane, Ayumi Yamashita, Kensuke Tono, Yasumasa Joti, Tomoyuki Tanaka, Shigeki Owada, Toshi Arima, Osamu Nureki, So Iwata, Gisela Brändén, Richard Neutze.
"Lipidic cubic phase serial femtosecond crystallography structure of a photosynthetic reaction centre" *Manuscript* (2019)

**Paper III:** Robert Dods*, **Petra Båth***, David Arnlund, Hoi Ling Luk, Robert Bosman, Kenneth R. Beyerlein, Garrett Nelson, Mengling Liang, Despina Milathianaki, Joseph Robinson, Rajiv Harimoorthy, Peter Berntsen, Erik Malmerberg, Linda Johansson, Rebecka Andersson, Sergio Carbajo, Elin Claesson, Chelsie E. Conrad, Peter Dahl, Greger Hammarin, Mark S. Hunter, Chufeng Li, Stella Lisova, Antoine Royant, Cecilia Safari, Amit Sharma, Garth J. Williams, Cecilia Wickstrand, Oleksandr Yefanov, Jan Davidsson, Daniel P. DePonte, Sébastien Boutet, Anton Barty, Gerrit Groenhof, Gisela Brändén, Richard Neutze.
**These authors contributed equally.* "Ultrafast structural changes in photosynthetic reaction centres visualized using XFEL radiation" *Manuscript* (2019)

**Paper IV:** Rebecka Andersson[*], Cecilia Safari[*], **Petra Båth**, Robert Bosman, Anastasya Shilova, Peter Dahl, Swagatha Ghosh, Andreas Dunge, Rasmus Kjeldsen Jensen, Jie Nan, Robert L. Shoeman, R. Bruce Doak, Uwe Müller, Richard Neutze, Gisela Brändén.
[*]*These authors contributed equally.* "Well-based crystallization of lipidic cubic phase microcrystals for serial X-ray crystallography experiments" *Manuscript* (2019)

**Paper V:** Rebecka Andersson, Cecilia Safari, Robert Dods, Eriko Nango, Rie Tanaka, Ayumi Yamashita, Takanori Nakane, Kensuke Tono, Yasumasa Joti, **Petra Båth**, Elin Dunevall, Robert Bosman, Osamu Nureki, So Iwata, Richard Neutze, Gisela Brändén.
"Serial femtosecond crystallography structure of cytochrome c oxidase at room temperature" *Scientific Reports* (2017)
doi: 10.1038/s41598-017-04817-z

Related papers that I have co-authored but that are not included in this thesis:

**Paper VI:** Przemyslaw Nogly, Daniel James, Dingjie Wang, Thomas A. White, Nadia Zatsepin, Anastasya Shilova, Garrett Nelson, Haiguang Liu, Linda Johansson, Michael Heymann, Kathrin Jaeger, Markus Metz, Cecilia Wickstrand, Wenting Wu, **Petra Båth**, Peter Berntsen, Dominik Oberthuer, Valerie Panneels, Vadim Cherezov, Henry Chapman, Gebhard Schertler, Richard Neutze, John Spence, Isabel Moraes, Manfred Burghammer, Joerg Standfuss, Uwe Weierstall.
"Lipidic cubic phase serial millisecond crystallography using synchrotron radiation" *IUCrJ* (2015)
doi: 10.1107/S2052252514026487

**Paper VII:** Przemyslaw Nogly, Valerie Panneels, Garrett Nelson, Cornelius Gati, Tetsunari Kimura, Christopher Milne, Despina Milathianaki, Minoru Kubo, Wenting Wu, Chelsie Conrad, Jesse Coe, Richard Bean, Yun Zhao, **Petra Båth**, Robert Dods, Rajiv Harimoorthy, Kenneth R. Beyerlein, Jan Rheinberger, Daniel James, Daniel DePonte, Chufeng Li, Leonardo Sala, Garth J. Williams, Mark S. Hunter, Jason E. Koglin, Peter Berntsen, Eriko Nango, So Iwata, Henry N. Chapman, Petra Fromme, Matthias Frank, Rafael Abela, Sébastien Boutet, Anton Barty, Thomas A. White, Uwe Weierstall, John Spence, Richard Neutze, Gebhard Schertler, Jörg Standfuss.
"Lipidic cubic phase injector is a viable crystal delivery system for time-resolved serial crystallography" *Nature Communications* (2016)
doi: 10.1038/ncomms12314

**Paper VIII:** Przemyslaw Nogly, Tobias Weinert, Daniel James, Sergio Carbajo, Dmitry Ozerov, Antonia Furrer, Dardan Gashi, Veniamin Borin, Petr Skopintsev, Kathrin Jaeger, Karol Nass, **Petra Båth**, Robert Bosman, Jason Koglin, Matthew Seaberg, Thomas Lane, Demet Kekilli, Steffen Brünle, Tomoyuki Tanaka, Wenting Wu, Christopher Milne, Thomas White, Anton Barty, Uwe Weierstall, Valerie Panneels, Eriko Nango, So Iwata, Mark Hunter, Igor Schapiro, Gebhard Schertler, Richard Neutze, Jörg Standfuss.
"Retinal isomerization in bacteriorhodopsin captured by a femtosecond x-ray laser" *Science* (2018)
doi: 10.1126/science.aat0094

**Paper IX:** Eriko Nango, Antoine Royant, Minoru Kubo, Takanori Nakane, Cecilia Wickstrand, Tetsunari Kimura, Tomoyuki Tanaka, Kensuke Tono, Changyong Song, Rie Tanaka, Toshi Arima, Ayumi Yamashita,

Jun Kobayashi, Toshiaki Hosaka, Eiichi Mizohata, Przemyslaw Nogly, Michihiro Sugahara, Daewoong Nam, Takashi Nomura, Tatsuro Shimamura, Dohyun Im, Takaaki Fujiwara, Yasuaki Yamanaka, Byeonghyun Jeon, Tomohiro Nishizawa, Kazumasa Oda, Masahiro Fukuda, Rebecka Andersson, **Petra Båth**, Robert Dods, Jan Davidsson, Shigeru Matsuoka, Satoshi Kawatake, Michio Murata, Osamu Nureki, Shigeki Owada, Takashi Kameshima, Takaki Hatsui, Yasumasa Joti, Gebhard Schertler, Makina Yabashi, Ana-Nicoleta Bondar, Jörg Standfuss, Richard Neutze, So Iwata.
"A three-dimensional movie of structural changes in bacteriorhodopsin" *Science* (2016)
doi: 10.1126/science.aah3497

**Paper X:** Petra Edlund*, Heikki Takala*, Elin Claesson, Léocadie Henry, Robert Dods, Heli Lehtivuori, Matthijs Panman, Kanupriya Pande, Thomas White, Takanori Nakane, Oskar Berntsson, Emil Gustavsson, **Petra Båth**, Vaibhav Modi, Shatabdi Roy-Chowdhury, James Zook, Peter Berntsen, Suraj Pandey, Ishwor Poudyal, Jason Tenboer, Christopher Kupitz, Anton Barty, Petra Fromme, Jake D. Koralek, Tomoyuki Tanaka, John Spence, Mengning Liang, Mark S. Hunter, Sebastien Boutet, Eriko Nango, Keith Moffat, Gerrit Groenhof, Janne Ihalainen, Emina A. Stojković, Marius Schmidt, Sebastian Westenhoff.
**These authors contributed equally.* "The room temperature crystal structure of a bacterial phytochrome determined by serial femtosecond crystallography" *Scientific Reports* (2016)
doi: 10.1038/srep35279

**Paper XI:** Jennie Sjöhamn, **Petra Båth**, Richard Netuze, Kristina Hedfalk.
"Applying bimolecular fluorescence complementation to screen and purify aquaporin protein:protein complexes" *Protein Science* (2016)
doi: 10.1002/pro.3046

**Paper XII:** Camilo Aponte-Santamaría, Gerhard Fischer, **Petra Båth**, Richard Neutze, Bert L. de Groot.
"Temperature dependence of protein-water interactions in a gated yeast aquaporin" *Scientific Reports* (2017)
doi: 10.1038/s41598-017-04180-z

# Contribution

**Paper I:** I did the protein purification and developed the crystallization protocol. I also went to all three experiments and did sample preparation and on-site processing of data.

**Paper II:** I did the protein purification and developed the crystallization protocol. I went to the experiment and collected data. I processed the data and prepared the manuscript.

**Paper III:** I did the purification and crystallization. I went to the experiments and did sample preparation and on-site processing of data. I did the refinement of the excited state structures and was involved in preparing the manuscript.

**Paper IV:** I was involved in developing the crystallization method. I was at the experiment and collected data.

**Paper V:** I was at the experiment and prepared the samples.

# Abbreviations

Here follows a list and short explanation of the different abbreviations used in this thesis.

| | |
|---|---|
| **ATP** | adenosine triphosphate |
| **BChl** | bacteriochlorophyll |
| **BPhe** | bacteriopheophytin |
| **CSPAD** | Cornell-SLAC Pixel Array Detector |
| **CXI** | Coherent X-ray Imaging |
| **EDTA** | ethylenediaminetetraacetic acid |
| **FNR** | ferredoxin-$NADP^+$ reductase |
| **FTIR** | fourier transform infrared spectroscopy |
| **GVDN** | gas dynamic virtual nozzle |
| **H123T** | heptane-1,2,3-triol |
| **LC** | liquid chromatography |
| **LCLS** | Linac Coherent Light Source (Palo Alto, USA) |
| **LDAO** | lauryldimethylamine oxide (N,N-dimethyldodecan-1-amine oxide) |
| **LCP** | lipidic cubic phase |
| **LH** | light harvesting protein |
| **LSP** | lipidic sponge phase |
| **MAG** | monoacyl glycerol |
| **MO** | monoolein (2,3-dihydroxypropyl (Z)-octadec-9-enoate) |
| **MPCCD** | multi-port charge-coupled device |
| **MQ** | menaquinone |
| **$NADP^+$/NADPH** | nicotinamide adenine dinucleotide phosphate |
| **P960** | The special pair of chlorophylls absorbing light at 960 nm |
| **PDB** | Protein Data Bank |
| **PEG** | polyethylene glycol |
| **PSI** | photosystem I |
| **PSII** | photosystem II |
| **RC** | reaction center |
| **$RC_{Vir}$** | reaction center from *Blastochloris viridis* |
| **$RC_{Sph}$** | reaction center from *Rhodobacter sphaeroides* |
| **SACLA** | SPring-8 Angstrom Compact free electron LAser (Hyogo, Japan) |
| **SFX** | serial femtosecond crystallography |
| **TR** | time resolved |
| **$Q_A$** | The primary quinone acceptor in PSII-type reaction centers |

| | |
|---|---|
| **$Q_B$** | The secondary quinone acceptor in PSII-type reaction centers |
| **UQ** | ubiquinone |
| **$UQ_2$** | ubiquinol |
| **XFEL** | X-ray free-electron laser |
| | |
| ***Bl. vir.*** | *Blastochloris viridis* |
| ***E. coli*** | *Escherichia coli* |
| ***Rh. sph.*** | *Rhodobacter sphaeroides* |

# Contents

# Chapter 1

# Introduction

## 1.1 Membrane proteins

Membrane proteins play a vital role in biological systems, where they are involved in a variety of functions including relaying extra-cellular signals through the membrane or transporting ions and other small molecules. Because of their exposure to external signals over 50 % of commercial drugs target them,[1–3] yet much less is known about them than proteins found in solution. The reason for this is that they exist in the hydrophobic environment of a lipid bilayer, conditions that are not trivial to replicate in a laboratory setting. Increasing knowledge of how these proteins work and finding robust methods to test their function is of great value to the scientific community.

## 1.2 Photosynthesis

One of the most important set of reactions in nature are those which involve transforming sunlight to chemical energy, photosynthesis. Plants have developed a complex mechanism for doing this over millions of years in order to convert carbon dioxide and water into more complex hydrocarbons. There are two main parts of the photosynthetic cycle termed the light-dependent reactions and the light-independent reactions. The light dependent reactions are driven by photoexcitation of electrons leading to an electron transfer chain through the membrane. The process starts with the excitation of the special pair (P680) of chlorophylls in the membrane protein photosystem II (PSII). (680 refers to the wavelength of light in nm at which the chlorophylls absorb.) This photoexcitation event leads to a charge separated state through the transfer of an electron to a second chlorophyll, followed by further transfer to a pheophytin moiety, before finally reducing a plastoquinone (Q). After a second electron transfer this is fully reduced to a plastoquinol ($QH_2$) which then dissociates from the protein into the membrane. The $P680^+$ of PSII is one of the

strongest oxidants in nature and is reduced by oxidising water to oxygen. The electron then passes through a cytochrome b6f complex before reducing plastocyanin, a small membrane-bound protein on the lumen side of the membrane. This plastocyanin eventually reduces the P700 of photosystem I (PSI) after a second photon absorption has taken place, leading to a new charge separated state where the final electron acceptor is an iron-sulfur cluster. The electron transfer chain ends with the eventual reduction of $NADP^+$ (nicotinamide adenine dinucleotide phosphate) to NADPH by the soluble ferredoxin-$NADP^+$ reductase (FNR) in the stroma. During the electron transfer process through these membrane complexes a proton gradient is formed, which is subsequently used in the formation of adenosine triphosphate (ATP) by ATP synthase. These "high-energy" molecules produced in the light reactions are then consumed in the light independent-reactions, which convert carbon dioxide into various hydrocarbons.[4,5]

## 1.3 Purple photosynthetic bacteria

Purple photosynthetic bacteria are organisms that can harvest light in order to create energy in a way that is very similar to photosynthesis in plants, with the bacterial reaction centers (RCs) being homologues of PSI and PSII. What distinguishes their photosynthetic system from plants is that the electron donor differs from water and they therefore do not produce oxygen. Instead, some of these bacteria use sulphur as an electron donor while others reuse their electrons in a process of cyclic electron transfer, which is the case for *Blastochloris viridis* (*Bl. vir.*) that the work in this thesis is based on (figure 1.1).[4] The ability of *Bl. vir.* to express photosynthetic proteins enables the species to live in anoxygenic environments, giving them an advantage in places such as deep lakes where they can absorb the light of longer wavelengths.[6] The presence of other cofactors in the photosynthetic proteins of different species, such as carotenoids, allow the bacteria to further fine-tune which wavelength of light to absorb, depending on the environment they live in.

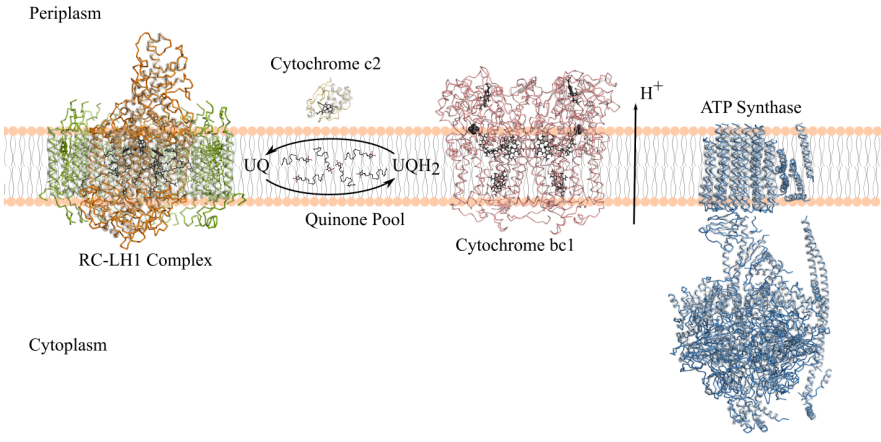


**Figure 1.1:** The proteins involved in creating the proton gradient in *Bl. vir.* Photons are absorbed by the RC or the surrounding LH proteins leading to an excited state that is energetically transferred to the P960 of the RC. The RC initiates an electron transfer chain leading to the reduction of a ubiquinone to ubiquinol that dissociates into the membrane to be oxidized again by the cytochrome $bc_1$ complex. The electron is shuffled through this complex before it is returned to the RC through cytochrome $c_2$. This cycle of electron passages leads to the buildup of a protein gradient utilized by ATP synthase.

*Bl. vir.* employ a simple two-part system for converting sunlight to energy. The first part is the RC which is surrounded by 17 light harvesting (LH) proteins.[7,8] The LH protein ring function as antennae that can direct the photons to the RC, initiating an electron transfer chain. Two electrons are eventually transferred onto a mobile ubiquinone (UQ) which acts as electron acceptor and additionally takes up two protons from the cytoplasm as it is reduced. The quinone can then diffuse into the membrane as ubiquinol ($QH_2$) and the electrons are transferred to a cytochrome $bc_1$ complex where the ubiquinol is oxidised again. The electrons are eventually returned to the RC through a cytochrome $c_2$ protein thereby completing the cycle.[9] Each passage of two electrons leads to the transport of four protons across the membrane into the periplasm; two from the reduction and oxidation of UQ and two from transporting the electrons through the cytochrome $bc_1$ complex. This formation of a protein gradient is what then fuels the synthesis of ATP.[10]

### 1.3.1 Reaction center

The RC from *Bl. vir.* ($RC_{Vir}$) was the first membrane protein structure solved by X-ray crystallography, work that was eventually awarded with a Nobel Prize.[11,12] This membrane protein together with the RCs from other bacteria, among them *Rhodobacter sphaeroides* ($RC_{Sph}$),[13,14] have been extensively studied to elucidate the mechanism of photosynthesis as the core structure of cofactors is very similar to that of PSII in plants. $RC_{Vir}$ consists of four subunits; the L and M subunits consist of five helices each (A-E) which hold the cofactors where the main electron transfer takes place, the H-subunit caps the protein on the cytoplasmic side and the C-subunit is a cytochrome on the periplasmic side containing four haem cofactors. The L, H and M notation stems from the "low", "medium" and "high" bands as the subunits appear during gel electrophoresis. $RC_{Sph}$ has a similar core structure but lacks the C-subunit. The absorption of photons takes place at a special pair of bacteriochlorophylls (P960). This leads to a charge separated state whereby an electron is transferred from P960 along the other cofactors of the L-subunit (also termed the A-branch); a second bacteriochlorophyll ($BChl_L$), a bacteriopheophytin ($BPhe_L$) and finally the primary quinone ($Q_A$), which in $RC_{Vir}$ is a menaquinone-9 (MQ). Before the charge separated state has a chance to collapse, the $P960^+$ is reduced by the closest heme in the C-subunit.[15,16] The electron then transfers from $Q_A$ to the mobile quinone site ($Q_B$) via a non-haem iron, together with a proton from water channels in the H-subunit.[17,18] (In $RC_{Vir}$ a ubiquinone-9 occupies the $Q_B$ site.) A second photon absorption then completes the formation of $QH_2$.[19]

### 1.3.2 Studies of electron transfer

A notable aspect of RCs with a quinone as final electron acceptor (such as $RC_{Vir}$ and PSII) is that the cofactors have an apparent $C_2$-symmetry but the electron transfer only takes place along one branch due to structural differences as the L- and M-subunits are not true homologues. The reason for deactivating one of the branches is unknown, but assuming that both pathways were possible it is reasonable that this limitation exists to make the transfer process as efficient as possible;[20,21] if both quinones could release from their binding sites simultaneously there is a chance that electrons would end up in an empty pocket, effectively nullifying the energy gained from photon absorption. It was theorized before the structures were known that bacterial and plant RCs had similar structures due to them displaying similar spectroscopic properties. In fact, before the structure of PSII had been solved the core structure of cofactors could be predicted based on the $RC_{Vir}$ structure,[22] and because of their similarities it is hypothesized that they are genetically linked.[23,24] This property, together with the simplicity of producing large amount of protein, makes bacterial RCs excellent targets for studying photosynthetic reactions and

elucidating the structural details of electron transfer. The first step was to establish the kinetics of the electron transfer as the first transfer from P960 to the $BPhe_L$ takes place in only 2.8 ps.[25,26] Initially it was believed that the electron bypassed the $BChl_L$[27] and it was termed an "accessory chlorophyll". However, it was later discovered that the $BChl_L$ is actually the first electron acceptor with a short-lived intermediate of less than 1 ps before the electron is passed on to the $BPhe_L$.[28–30] From the $BPhe_L$ to the $Q_A$ it then takes another 200 ps for electron transfer, followed by the reduction of $Q_B$ in another 100 µs.[18,31] After protonation and the passage of a second electron the $Q_B$ is fully reduced.

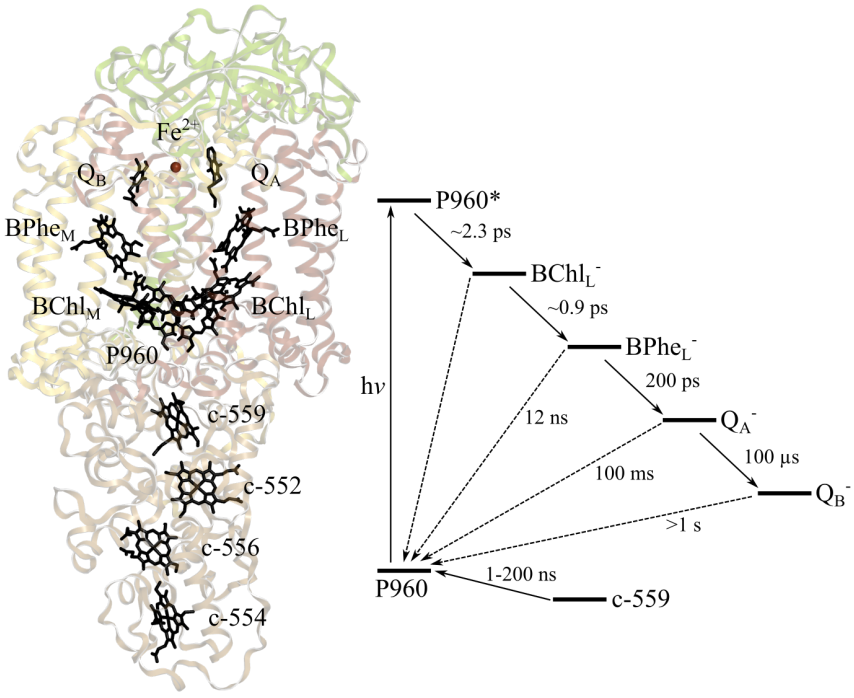


**Figure 1.2:** Position of cofactors in $RC_{Vir}$ as well as approximate time points of electron transfer between the cofactors after photon absorption at P960 for the first reduction of $Q_B$. The energy levels depicted are arbitrary. The tails of some cofactors are truncated for clarity.

The reduction potentials of the cofactors when situated within the protein are quite different compared to when they are in free solution.[18] The central question is whether electron transfer is taking place inside a static structure where the environment of the cofactors is modulating these reduction potentials, or if the protein

can also respond to photon absorption with movement and thereby "control" the process. One example of this type of movement is the theory proposed by Stowell et al. that the UQ moves further into the $Q_B$ binding pocket by approximately 4.5 Å upon illumination, assuming a proximal position similar to the MQ in the $Q_A$ binding pocket. This has been indicated in experiments using $RC_{Sph}$ and would thereby constitute a gated transfer where the UQ cannot be reduced if the protein is kept dark and remains in the distal position.[32] This theory has since been disputed both by Fourier transform infrared (FTIR) difference spectroscopy[33] and additional crystallographic experiments in $RC_{Vir}$.[34] This is discussed further in **Paper II** but it is reasonable that the UQ will assume different positions as it moves in and out of the membrane and only the intermediate semi-quinone is expected to stay in the $Q_B$ pocket in order to be fully reduced.[35]

Large movements such as that postulated for UQ are easily distinguishable when the structure is determined, however the same cannot be said for the initial charge separation and electron transfer from the P960 to the $Q_A$. Marcus theory on electron transfer, based on the distance between the cofactors and activation energies, predicts reaction kinetics similar to experimental results.[36,37] This indicates that the electron can transfer between the cofactors as long as the orbitals overlap in energy. In $RC_{Vir}$ the initial charge separation between P960 and $Q_A$ is close to barrier-less, making it an extremely efficient process (The quantum yield of photon absorption is close to 100 %.[38]) The collapse of the charge separated state, although thermodynamically favoured, is prevented by being in the so called "inverted region" where an increase in the driving force of the reaction makes the reaction slower. This leads to subsequent electron transfer steps taking place before the electron has a chance to return to $P960^+$. The collapse of the charge separated state is further hindered by the $P960^+$ being reduced by the closest heme of the C-subunit after 120 ns, blocking the return pathway.[16] Studies on temperature effects showed that the electron transfer rate from the P960 to the $BPhe_L$ is actually sped up by lower temperatures,[39] which would indicate cofactors being locked in a favourable position and refutes protein dynamics being part of the process. Nevertheless, there is still debate about whether or not there are additional smaller movements in the protein that influence these electron transfers. In fact, other studies do indicate that protein dynamics have a role. One notable spectroscopic study on $RC_{Sph}$ mutants showed that the mechanics of the initial charge separation was the same for all mutants independent on reaction kinetics, this was explained by structural changes in the protein upon photon absorption affecting the initial electron transfer.[40]

## 1.4 Scope of this thesis

This thesis focuses on the production and crystallization of $RC_{Vir}$ with the goal of studying its function and the detailed structural changes occurring upon photoexcitation. The method used is serial femtosecond crystallography (SFX) which requires thousands of crystals measuring less than ~25 μm in size. **Paper I**, **Paper II**, **Paper IV** and **Paper V** present new ways of crystallizing protein for SFX experiments where protocols have been developed to generate homogeneous crystals and larger sample volumes. The results of the crystallization is discussed in chapter 4, while the structural details of protein structures from these crystal forms are presented in chapters 5 and 6. **Paper III** presents a time resolved study on one of these crystal forms at an X-ray free-electron laser (XFEL), looking into the structural changes of $RC_{Vir}$ in two of the primary electron transfer steps to the $BPhe_L$ and the MQ.

# Chapter 2

# Methodology

When studying proteins it is imperative to ensure that observations stem from the protein itself and not simply as a result of of its unnatural surroundings. Usually, a host organism is used to produce the protein which introduces the complication that the target protein must be separated from all of the many thousands of macromolecules present in the host cells. Furthermore, while crystallization in itself is a technique for purifying molecular compounds, proteins usually need to already be fairly pure in order to produce crystals at all. Once obtained the crystals can be used for structural determination by X-ray crystallography and time resolved studies by looking at the difference between several sets of structural data.

## 2.1 Membrane protein purification

Compared to soluble proteins membrane proteins have been a more elusive target for structure determination. First of all, very few of them are abundant in their natural source and need to be overexpressed recombinantly. This is a more difficult process than with soluble proteins as they need to be inserted into a membrane during synthesis and folding inside the cell. Most proteins are more unstable in a buffer system rather than the natural environment of a living cell, but this problem is taken to an even further extreme with membrane proteins, as they need to be stripped from the membrane in order to get them into solution for purification. This makes them more unstable compared to soluble proteins as their large hydrophobic regions are more prone to aggregation. Stabilizing the protein can be achieved by keeping it cold during the purification, by adding protease inhibitors for proteases that would degrade the target protein or by buffer additives such as glycerol.[41]

### 2.1.1 Cell growth

For most membrane proteins recombinant expression is the dominant technique for production. Many parameters need to be optimized in order to obtain good levels of expression. Firstly, a suitable host cell need to be chosen. *Escherichia coli* (*E. coli*) is a well-known and simple system for producing high yields of protein, but not all eukaryotic proteins can be expressed in prokaryotic systems due to the lack of chaperones and post-translational modifications needed for stability. Furthermore, the lipids of the host membranes need to match the protein and the induction rate of expression needs to be optimized for proper insertion into the membrane.[42]

### 2.1.2 Solubilization and detergent effects

Following collection of the membranes, the target protein must be solubilized (see general process of dissolving a membrane in figure 2.1). There are a number of detergents available and often a screen is needed to determine which one is the most suitable for the protein. Detergents generally have a core structure of a hydrophilic head group and a lipid tail that allow them to form micelles in solution but they all have individual properties that need to be taken into account when purifying and crystallizing. Detergents are considered mild or harsh mostly depending on the charge of the head group. Non-ionic detergents tend to only disrupt lipid-protein interactions and ionic detergents can disrupt protein-protein interactions even going so far as denaturing the protein. Each detergent also has a unique aggregation number (the number of molecules in a micelle) and critical micelle concentration (the concentration needed for a micelle to form). These properties need to be taken into account when designing buffers or using molecular cut-off filters. Depending on what the protein will be used for once it is purified you may want to strip away the detergent or exchange it for a different lipid. In that case, it is important to purify the protein in a detergent that is easy to remove later on, as some detergents tend to bind to proteins more tightly.[43]

### 2.1.3 Chromatography

Once the protein is in solution one or more liquid chromatography (LC) steps are performed to purify it using the unique properties of the protein to separate it from other macromolecules. Most methods employ columns consisting of a resin in a buffer system, which is then attached to an automated LC system that can pump liquid onto the column. The protein solution is loaded onto the column and eluted into fractions after separating it from other components. Ion-exchange (IE) chromatography utilizes the net charge of the protein to make it bind to a positively or negatively charged resin. It is then eluted by increasing the salt concentration or by

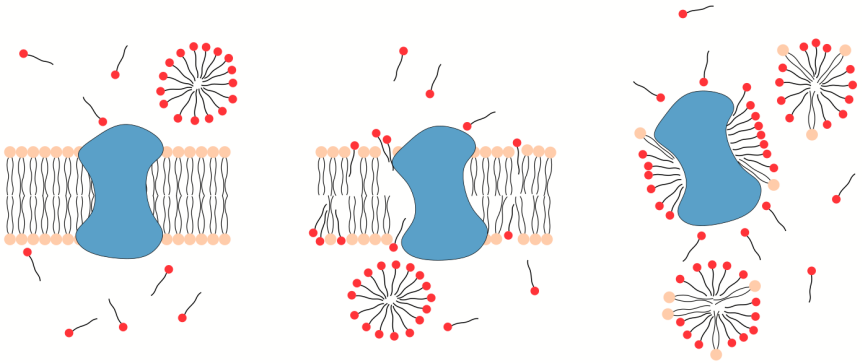

**Figure 2.1:** Using detergent to dissolve a lipid bilayer and solubilize the protein situated within it. With an excess of detergent molecules they will eventually replace the native lipids around the membrane region of the protein as the bilayer dissolves.

changing the pH of the buffer. Affinity chromatography is another method where, in theory, only the protein of interest can bind to the resin. Many membrane proteins are purified this way by genetically attaching a poly-histidine tag that can bind to a nickel- or cobalt-resin, which is then eluted by addition of imidazole or lowering the pH.[44] In reality there is often also some degree of unspecific binding to the resin by other proteins but the overall purity is still improved by a major degree.

If the purity is not high enough the last step of a purification is usually size exclusion chromatography (SEC). This simply resolve the proteins in the solution by size as they pass through the column and is a good way to check the integrity of the sample as a pure protein optimally will elute as a bell-curve. SEC can also be used analytically to screen various buffers and detergents as the appearance of aggregates and oligomers can be seen in the elution profile. Proteins with large detergent micelles will affect the total protein-detergent complex size and migrate faster through the column so it is important to not choose the resin only depending on the protein size but to also take the detergent into account.

### 2.1.4 Purification of $RC_{Vir}$

$RC_{Vir}$ is relatively easy to produce, since large amounts can be expressed in its host cell *Bl. vir.* by incubating in dark and light cycles to induce expression of the photosynthetic proteins. The cells are then collected and disrupted by sonication to

extract the photosynthetic membranes where the RC is located.[45] $RC_{Vir}$ is solubilized in lauryldimethylamine oxide (LDAO), a zwitterionic detergent that has been used to purify RCs since the first protocols were developed. After solubilization the membranes are removed by centrifugation and the protein is purified by IE and SEC chromatography. The concentration and purity of the protein is determined by UV-Vis spectroscopy. The concentration is measured at at 830 nm which corresponds to the absorption for P960 and the BChls.[46] The purity is determined as the ratio of 280 nm (the absorption of aromatic amino acids of all proteins in the solution) and 830 nm. For studies in solution a purity of 2.3-2.5 is sufficient, but for crystallization it is optimal to be at 2.2 or lower.

## 2.2 Crystallization

A crystal is formed when protein molecules can be convinced to arrange themselves in an orderly array. This usually involves a lot of time and effort spent, first on purifying the protein to make sure it is homogeneous, then screening an endless amount of possible crystallization conditions in order to find one or more that works. There are several ways to crystallize proteins but one of the most common methods is by vapour diffusion.[47,48] In a vapour diffusion setup a drop of the protein is mixed with a drop of reservoir solution containing a precipitant, the drop is then sealed in a chamber together with the reservoir. Since the protein drop has a lower molecule content it will lead to the migration of water molecules from the protein drop to the reservoir, thereby supersaturating the protein solution. With proper conditions crystals will then begin to form and continue to grow until equilibrium is reached. The outcome is very much dependent on the concentrations of both the protein and the precipitant and is usually represented like the diagram in figure 2.2.[49] Initially you move from the lower-left towards the upper-right corner as both the concentrations of the protein and precipitant are increasing as the water molecules evaporate. In the nucleation zone the first protein molecules start to organize themselves into an ordered structure and as they continue to build the crystal the protein concentration drops until it reaches equilibrium in the metastable zone. However, in reality the process is not that simple and the most likely outcome is that the protein instead precipitates as it is energetically more favoured in the short-term. Another common method for crystallizing is batch crystallization where instead of equilibrating the drop against a reservoir solution you simply mix the protein with a precipitant in order to get a supersaturated solution from the setup of the drop.

In the beginning of screening for crystals it is common to set up multi-well plates with a pipetting robot. A robot enables high throughput screening of many conditions and keeps the sample consumption down. There are various commercial

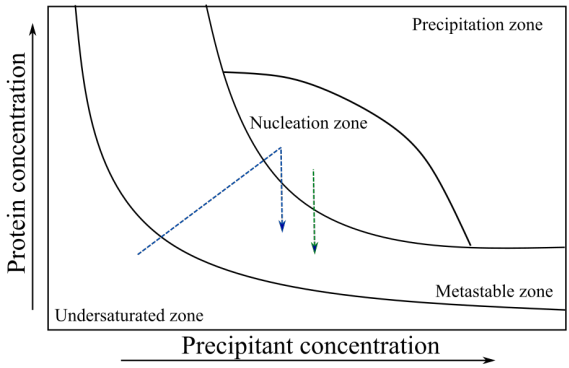


**Figure 2.2:** Phase diagram of a typical crystallization setup. The blue arrow represents a vapour diffusion setup and the green arrow represents a batch setup.

screens available, often marketed to certain types of proteins based on published structures. Initial screening usually involves varying pH and testing different salts and small-molecule precipitants like polyethylene glycols (PEGs). Once crystal hits have been found it is usually followed by optimization around the conditions to produce the best crystal possible by varying concentrations of the different crystallization components or finding an additive that improves crystal growth.

Crystal quality is the main parameter that determines the quality of the data possible to extract from it. The rate of crystal growth often has an impact on final quality of the crystal to some extent so it is common to grow crystals at lower temperatures or find conditions that slow down crystal growth. (The effect of temperature on $RC_{Vir}$ crystals can be seen in chapter 4.) You can also combine this with seeding protein drops with previously grown crystals to introduce a nucleation site for a better crystal to grow. In some cases it is necessary to spend more time on protein engineering to make the protein more suitable for crystallization. This can include removing affinity tags used in purification that may block crystal contacts, removing flexible regions such as terminal tails or adding specific antibodies to the protein during crystallization.[50,51] When crystallizing membrane proteins the detergent micelle has to allow the protein to make crystal contacts. A very common additive to crystallization setups of RCs is heptane-1,2,3-triol (H123T) which has been shown to remove some of the LDAO molecules from the protein-detergent micelle thereby making it easier for the protein to crystallize.[52]

It is easy to imagine that a crystal is made up of pure protein but a large percent of the mass of a crystal is comprised of water. This enables ions and small molecules in the precipitant solution to interact with the protein. The crystal can also be soaked in different solutions, for example to study ligand binding effects or to apply a cryo-protectant before freezing.

### 2.2.1 Lipidic cubic phase

For crystallizing membrane proteins there is an added challenge as they are protected by their detergent micelles in solution; it makes the number of possible initial crystal contacts fewer and when the detergent lipids are stripped away the proteins are more prone to aggregating. For that reason lipidic cubic phase (LCP) has been developed as a crystallization method for membrane proteins as it provides a more natural environment.[53] It consists of a mixture of a lipid and water that are mixed in glass syringes until homogeneous. There are a number of different phases the mixture can assume depending on the ratio of lipid to water, ranging from solid bi-lamellar to completely liquid. The LCP phase is unique because it is a soft solid, almost toothpaste-like in consistency. The lipids form a continuous bilayer much like a membrane for the protein molecules to sit in, at the same time it is filled with water pores which allow different solutions to penetrate the solid. It is also transparent which permits monitoring of the crystallization progress. When crystallizing with the LCP method you first mix the protein solution with a lipid, usually melted monoolein which is a monoacylglycerol (MAG). (This is also called MAG9.9 where the numbers denote the number of carbons in the acyl chain before and after the double bond to differentiate it from other MAGs.) The LCP is then suspended in a precipitant solution, either in a sealed well or by injecting it into a larger glass syringe. While monoolein is the "standard" many other lipids can be used as additives or by themselves to make conformational changes in the LCP or to match the size of the target protein better.[54] If applicable the natural membrane lipids for the protein can be doped into the LCP as well as components with low solubility in water such as cholesterol.[55] If the protein that is being crystallized is a membrane protein it is also important to note that detergents will also affect the properties of the cubic phase to some extent.[56]

Precipitants in crystallization setups also have an effect on the structure of the LCP, especially PEGs and alcohols. At the right concentration they make the water pores in the LCP slightly larger which gives more room for protein domains outside the membrane region, but if the concentration is too high it instead melts the LCP into an oil. This is the swollen form of LCP called lipidic sponge phase (LSP). Contrary to LCP, LSP is mixed from buffer without the protein where additives such as PEG or Jeffamine turn the lipid mixture into a less viscous state. This can then be

used for crystallization by itself mixed with the protein solution or as an additive in vapour diffusion setups.[57,58]

One drawback of crystallizing in LCP is that it is temperature dependent. At higher temperatures it will transition into a different phase and become more liquid. More troublesome though is that below room temperature at roughly 18 °C it will solidify. This means that growing crystals at a low temperature is generally an option that is unavailable unless specialized lipids are used. In most cases the crystals are fished from the LCP, optionally dissolving the cubic phase before fishing,[59] and flash frozen before transport. However, in experiments where crystals are needed inside the LCP the temperature dependence adds a layer of difficulty in transporting and shipping the sample at room temperature.

## 2.3 X-ray diffraction and data collection

In 1913, Lawrence Bragg and his father William Bragg discovered that illuminating crystalline materials with X-rays produced patterns arising from the incoming beam being reflected on atomic planes in the crystal structure.[60] This discovery led them to the derivation of Bragg's law and serves as the fundamental of protein structure determination by X-ray crystallography. When X-rays interact with atoms the electrons respond by scattering some of the incoming beam. If they are ordered as in a crystal the reflected X-rays will interact by constructive or destructive interference giving a diffraction pattern. Constructive interference is given by Bragg's law:

$$n\lambda = 2dsin\theta \tag{2.1}$$

where n is a positive integer, $\lambda$ the wavelength of the incoming X-ray, d the spacing between two lattice planes and $\theta$ the scattering angle. The spots making up a diffraction pattern are also referred to as reflections from viewing the crystal as a mirror that can reflect the X-rays.

The symmetry of the crystal lattice is also reflected in reciprocal space and the Ewald sphere (figure 2.3) can be used to predict when constructive interference will occur depending on the wavelength of the X-ray and the space group of the crystal.[61] Every time a reflection point in reciprocal space intersects with the Ewald sphere that reflection can be measured. Therefore, when collecting data the crystal will be rotated along one axis in order to sample all of the reciprocal space. An analogy to this would be stepping outside on a starry night, then facing the same direction different constellations will come into view as time passes and the Earth spins around its axis. How far the crystal needs to be rotated depends upon the symmetry of the crystal with a low symmetry crystal needing a full 360 ° rotation.

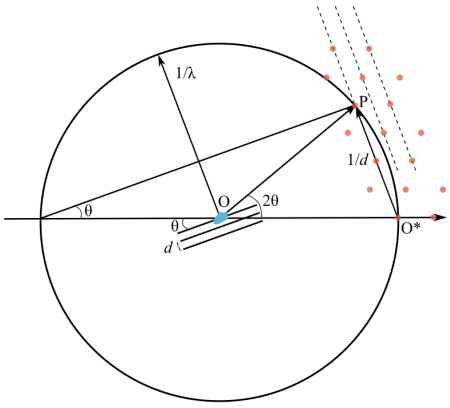


**Figure 2.3:** A 2D representation of the Ewald sphere showing the interaction with reciprocal space as an X-ray with wavelength $\lambda$ is reflected on crystal planes with distance d.

When crystals are irradiated with X-rays it also gives rise to free radicals that induce radiation damage and with time a crystal will lose its diffracting power. In crystallography it is often desirable to have large crystals since they have stronger reflections and are less prone to be affected by radiation damage allowing all of reciprocal space to be sampled.

### 2.3.1 Data processing and structure solving

Reflections are sorted by their Miller hkl indices by crystallographic software such as Mosflm[62,63] or XDS[64] according to the space group of the crystal. The reflections that are measured more than once are merged giving the redundancy or multiplicity of the data where a higher multiplicity gives a more accurate measurement of the reflection. Since the crystal lattice and reciprocal space both consist of repeating units it is possible to calculate the electron density of the crystal by a Fourier transform:

$$\rho(x,y,z) = \frac{1}{V}\sum_{x}\sum_{y}\sum_{z} F(hkl,xyz) \tag{2.2}$$

$$F_{hkl} = |F_{hkl}|e^{i\alpha hkl} = \sum_j f_j e^{2\pi i(hx_j + ky_j + lz_j)} \tag{2.3}$$

Where $\rho$ is the electron density of the atoms in the unit cell (the smallest repeating unit in the crystal) and $F_{hkl}$ is the structure factor of the reciprocal lattice point hkl. The structure factor is in turn a sum of the scattering of all atoms j in the unit cell where $f_j$ is the atomic structure factor. The main difficulty going back to an atomic structure from reciprocal space is that the data lacks information about the phases ($\alpha$) of the wave functions and the diffraction patterns only contain information about the intensity of light that hit the detector, which is proportionate to the amplitude $|F_{hkl}|$. This is commonly known as the "phase problem", and as most of the structural information is contained in the phases these need to be obtained from somewhere else. Experimentally, phases can be obtained by heavy atom incorporation but this comes with some challenges. In isomorphous displacement, crystals with and without heavy atoms are measured, but the data cannot be compared unless the crystals are exactly the same with no changes in the unit cell parameters. In anomalous dispersion, the wavelength of the X-rays is changed to also collect data at the absorption edge of a scattering atom and the same crystals can be used, but then there is an increased chance of radiation damage due to the higher dosage.

Molecular replacement obtains theoretical phases from an input model that is structurally similar to your target protein and is the most common method to calculate the initial phases for a structure. The first step is a Patterson function:[65]

$$\rho(u, v, w) = \sum_{hkl} |F_{hkl}|^2 e^{-2\pi i(hu + kv + lw)} \tag{2.4}$$

The Patterson function is mainly used in direct methods to determine atomic positions in small molecules. By omitting the phase the interatomic vectors can be calculated. Since the resulting signal is proportional to the atom number it is possible to start building a structure by finding the positions of the heaviest atoms. In a protein that contains thousands of atoms this is not possible, but the Patterson function is used in the first step of molecular replacement by some crystallographic software, where the model of the protein is rotated as the first step of finding its position in the unit cell.

Once the initial structure has been found several iterations of building the model into the electron density takes place. These are followed by rounds of refinement in reciprocal space to improve the electron density map with the new phases from the model. Two maps are used for model building: the $2F_{obs}$-$F_{calc}$ map and the $F_{obs}$-$F_{calc}$ map. The $2F_{obs}$-$F_{calc}$ map shows the electron density that the model is built

into. Subtracting the calculated map from a multiple of the observed map instead of using only the observed map is done to further remove model bias. The $F_{obs}$-$F_{calc}$ map shows positive and negative peaks depending on if something is missing in the model or is in the wrong place. Since the phases of the model contribute so much to the structure it is important to avoid model bias, which means that you are building the wrong molecule into the electron density. One metric to look at is the $R_{work}$ value, it compares the difference of the calculated structure factors from the model to the observed structure factors:

$$R_{work} = \frac{\sum ||F_{obs} - F_{calc}||}{\sum |F_{obs}|} \tag{2.5}$$

This is usually given in a value of per cent and as the model converges to the experimental data it approaches 0 which would correspond to a perfect fit. When analysing real data this will never happen and a value of roughly ten times the resolution is deemed acceptable. If $R_{work}$ is too high it is likely that the model is not true where a value above ~0.6 corresponds to a random structure. As overfitting the model will make $R_{work}$ artificially low a subset of the data, usually 5-10 %, is left out of the refinement of the model to give the $R_{free}$ value. This will be slightly higher than $R_{work}$ and as long as they are close in value the model should be satisfactory. Another thing used to validate the structure is to make sure that it is chemically correct. This include bond lengths and angles as well as the torsion angles of the peptide bonds.[66–68]

# Chapter 3

# XFEL Data Collection and Pump-Probe Experiments

## 3.1 X-ray free-electron lasers

Most protein structures to date have been solved by X-ray crystallography at one of the many synchrotron sources available. One of the major advances with retaining good quality diffraction of crystals came with cryo-cooling to prevent radiation damage[69] and in addition to flash-cooling there are now many strategies for preserving crystals to collect data at 100 K.[70] Time resolved studies at synchrotrons have therefore relied on methods such as freeze-trapping crystals or Laue diffraction utilizing a polychromatic beam to measure many reflections simultaneously. Still, it is not possible to reach time points shorter than ~100 ps with third-generation synchrotrons.[71,72] XFELs make up the new generation of X-ray sources with brilliance a million times stronger than synchrotrons, pushing the limits of the diffraction possible from a crystal. Additionally, data is collected at room temperature, and with a pulse length in the span of femtoseconds it is also possible to do time resolved pump-probe experiments in the femtosecond regime.

### 3.1.1 XFEL delivery systems

Collecting crystallographic data at an XFEL is in essence the same as for crystallography performed at a synchrotron. As the brilliance of the X-ray will destroy the crystal it is impossible to rotate it in order to collect all the reflections needed to solve a structure. However, the electrons in the sample will still scatter the incoming beam before the crystal is destroyed by the radiation damage, this has become known as "diffraction before destruction".[73,74] Instead, an SFX methodology is employed where thousands of micro- to nanometre-sized crystals are subjected to the X-ray beam, either via a raster-scan of a solid support or more commonly by being injected into the beam in a stream of carrier media. The first sample injector

designed for SFX is the gas dynamic virtual nozzle (GDVN),[75] made for injecting crystals in solution. This injector consists of a nozzle with a 50-100 µm inner diameter that the sample is pushed through by the means of water from an LC pump. An He gas sheath around the tip of the nozzle helps the jet form a stable stream into the X-ray beam and many of the early XFEL structures used this delivery system. However, the high flow rate of the sample (around 10 µl/min or 10 m/s) means that most crystals will never be probed by the X-ray beam and it puts extreme demands on the amount of sample needed as several hundred milligrams of protein can be used for one experiment.

Several other injection systems[76,77] have been developed in order to slow down the flow rate of the sample injection and thereby reduce the sample volume. The one that has gained the most traction is the viscous injector that was initially developed for microcrystal samples grown in LCP.[78,79] The main function of the injector is the same as that for the liquid injector: an LC pump pushes the sample through a nozzle with the help of a sheath gas to direct the flow. The difference is that the flow rate is much slower which reduces sample consumption considerably. Typical consumption rates for structure determination are in the order of a few hundred nanolitres per minute.

There are some inherent issues with LCP as it is prone to shift phase both during crystallization due to high precipitant concentrations and during injection into a vacuum chamber as is the case at the LCLS. However, this can be circumfered by addition of other MAGs (monopalmitolein/MAG9.7 or MAG7.9) or changing the sheath gas used for the nozzle from He to $N_2$.[78,80] To use crystals grown by vapour diffusion or batch in the viscous injector there are now multiple carrier media[79,81–85] that have been developed as a substitution for the LCP. The crystals are simply mixed with the media and used as you would an LCP crystal sample. These alternatives usually display lower background-scattering (LCP has a distinguishable ring similar to the background scattering of water at ~4.5 Å) and are a valuable resource both for screening purposes and if growing crystals in LCP is not an option. However, fragile crystals might break during the mixing process and the carrier media are not always compatible with the high precipitant and salt concentrations used for crystallization. Furthermore, not all carrier media display the same non-Newtonian properties LCP has of becoming more liquid under pressure, which has consequences for how the sample behaves in the injector.[86]

There are still advantages to performing experiments in solution such as lower background scattering, the ease of studying light-activated proteins and the prospect of studying chemical reactions where substrates are mixed with the protein crystals. It is also possible to concentrate the crystals by removing some of the mother

liquor in order to increase the hit rate. Therefore, efforts are still ongoing to reduce the sample consumption and to create more specialized injectors.[87,88] The viscous injector is now being installed at several synchrotrons for structural determination and time-resolved experiments on the millisecond timescale, but it is now too slow for the higher repetition rates of some of the newer XFELs being built validating the need for efficient liquid injectors. (E.g. the European XFEL having a repetition rate of ~30 kHz and the upgrade of LCLS to LCLS-II aiming for a repetition rate in the MHz regime.) Both types of injectors have been used for the papers presented in this thesis. $RC_{Vir}$ is one of few membrane proteins easily produced in the quantities needed for an experiment with the liquid jet, on the other hand LCP provides the opportunity to perform different types of experiments.

### 3.1.2 Serial crystallography data processing

An SFX experiment gives thousands of diffraction patterns, considering the beam operating at 120 Hz at the LCLS this would theoretically give ~5 million frames for a normal 12 h shift. Therefore, specialized software has been developed to be able to sort through and merge the large amount of data from these experiments. The software used in this thesis are Cheetah and CrystFEL, where Cheetah is used for hit finding and CrystFEL for the indexing, scaling and merging of the reflections but there are several other software packages available. As many of the collected frames come from the X-ray hitting the jet when there is no crystal present the first step is to find which frames has diffraction spots. This is typically done by reading the pixels of the detector with the highest intensities and checking if they are above a defined signal-to-noise (SNR) ratio. If a frame has enough spots it is deemed to be a diffraction pattern and counted as a hit. The collected patterns are then indexed by implementing functions from standard software such as Mosflm[62,63] or XDS.[64] Usually, a subset of images are indexed first to determine the space group and unit cell of the crystals as well as optimising the spot finding and geometry of the detector panels, these parameters are then set to index the entire dataset.[89]

As each diffraction image corresponds to a unique crystal and because of fluctuations in the intensity and wavelength of the X-ray beam, there will be a lot of variation between the images that need to be taken into account. Before merging, all reflections are scaled to an average of all the patterns, there is also the option to further account for partial reflections by letting the Ewald sphere be represented by a broader value than that of a fixed wavelength. Improving the crystal geometry by a post-refinement step in between the scaling cycles generally improves the quality of the data.[90,91] After merging the reflections it is important to validate the data by comparing some figures of merit. In addition to completeness and SNR there are

some figures of merit based on the self-consistency within the dataset calculated by splitting it in half and comparing the two halves to each other. Some examples include the Pearson correlation coefficient (CC1/2), CC*[92] and Rsplit:

$$R_{split} = \frac{1}{\sqrt{2}} \frac{\sum |I_{even} - I_{odd}|}{\frac{1}{2} \sum (I_{even} + I_{odd})} \tag{3.1}$$

Even- and odd-numbered images are compared to each other and better data gives a lower value for $R_{split}$. Dividing by $\sqrt{2}$ aims to adjust the value to account for the fact that it only looks at half of the dataset. After merging, the data can be used for molecular replacement with Phaser[93] in CCP4[94] or Phenix[95] as any other crystallographic data. There is also ongoing work being done to do more anomalous dispersion experiments at XFELs in the future as this is the main technique for finding new types of protein structures.[96,97]

### 3.1.3 Pump-probe experiments and difference density maps

The large amount of data generated is not the only hurdle at an XFEL experiment. The fast repetition rate of the XFELs means that specialized detectors have been built for them to account for the faster readout times and higher radiation doses (they are built as panels to let the high-energy X-ray pass through the detector rather than relying on a beamstop).[98–100] For a time resolved experiment you also need to reliably align the laser with the sample flow and time it with the flow rate.[101,102] In addition to the hardware at the experimental setup, the intensity of the laser and how well it penetrates the crystal need to be considered. This will affect both the occupancy of the crystal (i.e. how many proteins in the crystal absorb light) as well as the number of photons absorbed by each protein. The laser power should be balanced so that it is high enough to generate an acceptable occupancy but not so high that the protein is quenched and non-linear effects begin to dominate the result. For $RC_{Vir}$ it has been shown that for higher laser powers heating of the protein adds to the structural movement of the protein.[103] In general, a higher laser intensity would be needed for the viscous jet as it is thicker and has a higher optical density.

When doing a time resolved experiment you look at the $F_{obs}$-$F_{obs}$ difference map between two different states of the protein. Since most experiments look at structures before and after laser activation this is also termed $F_{light}$-$F_{dark}$. Because this signal is weaker due to lower occupancy you would need to collect several times the amount of data which would be needed for structural determination alone. The exact amount varies and is usually monitored as the experiment progresses by calculating maps from the unrefined structure. At this point it is imperative to have

a high hit rate as it would allow the collection of data on several time points and make better use of XFEL beamtime. After refinement of the dark state structure the difference maps can then be improved by using the phases of the new model. The standard when interpreting difference maps is that the signal should be above 3.0 $\sigma$ with a strong signal being 3.5-4.0 $\sigma$. For large structural movements this is easily attainable but smaller structural movements will be closer to the noise level and therefore more difficult to interpret with the same level of confidence. There are efforts being made at improving this signal, for example in **Paper III** Bayesian statistics was used to amplify the signal in the difference map.[104]

# Chapter 4

# Microcrystallization for Serial Crystallography

In a standard X-ray experiment the aim is to get crystals as large as possible. A bigger crystal in general gives better data by having more reflections and is more resistant towards radiation damage. However, there are multiple applications where you want to have many small crystals instead. There are several injection systems at XFELs that rely on injecting crystals in a stream, collecting data from thousands of small crystals rather than from a few larger ones at a synchrotron. There are also several new systems being developed where crystals are loaded into multi-well plates or on microfluidic chips creating new possibilities for screening both at XFELs and synchrotrons.[105–107]

In many cases when you screen for large crystals you instead end up with many small crystals because of fast nucleation rates. Sometimes they disappear in favour of a few larger crystals due to Ostwald ripening, but if they are stable they can be used as is. Several XFEL structures have been solved from batch conditions[108] (including **Paper X**) and with a crystal hit from a vapour diffusion setup only a few parameters should have to be explored to find a possible batch setup.[109] One difficulty of working with microcrystals is that they are notoriously difficult to monitor with a standard light microscope and differentiating between crystalline material and precipitant can be near impossible. There have been some advances in image processing to identify crystal hits,[110] but other than that you have to rely on more expensive systems such as transmission electron microscopy[111] or simply hope that the crystals diffract once they are brought to an X-ray source.

## 4.1 Seeding for microcrystallization of $RC_{Vir}$

Previously, $RC_{Vir}$ has been crystallized for SFX studies in LSP. This crystal form was used with the GVDN at the LCLS and yielded some of the first XFEL structures at 8.2 and 3.5 Å respectively.[112,113] Unfortunately, it had some inherent problems that made it unsuitable to use for a time-resolved experiment. The low hit rate of only 0.2 % in those studies meant that a great amount of sample was needed to collect the necessary data. The problem with low amounts of data was pushed further by a unit cell with a c-axis measuring almost 400 Å, making the diffraction spots extremely difficult to separate. Because of this the final indexing rate was only about 20 % of confirmed patterns. For time resolved studies the strategy for the crystallization in **Paper I** and **Paper III** was therefore to move back to vapour diffusion setups. With lower supersaturation of the solution it is possible to dope it with a seed stock, this has the advantage of a more controlled growth and has been the key factor in generating well-diffracting crystals for $RC_{Vir}$ in the papers presented in this thesis.

The first crystallization condition was adapted from the original conditions[114] with a few minor changes. This gave rod-shaped crystals averaging around 200 µm in the longest dimension. In order to get these crystals to flow freely through the GVDN system which requires a sample size of less than 20 µm in all directions, a crushing protocol was developed to physically break the crystals into smaller pieces and these were used as is for the first LCLS experiment in 2014 (**Paper I**). The mechanical damage on the crystals could be seen in the diffraction patterns as spot streaking but the sample was still good enough for data collection. This method has also shown promise when applied to crystals of other proteins such as the bacterial phytochrome presented in **Paper X**. These crystals appear to take less damage from the crushing and the structure could be solved to 2.5 Å.

Instead of breaking macrocrystals by force we wanted to improve the crystallization conditions to generate microcrystals. Our first strategy was to grow them at 4 °C rather than at room temperature, this slowed crystal growth to 72 h instead of 24 h, and while they still grew to a similar size as before there was a visible improvement in quality were the crystals had sharper edges (compare figure 4.1 top left and top right). The next strategy employed seeding as a way to further tweak the nucleation process of the crystallization conditions. Seeding is a common technique in crystallization and in theory allows lowering the precipitant concentration, leading to a slower growth rate and eventually a more highly ordered crystal.[115] Less concentrated solutions also lower the risk of protein aggregation. Using the crushed crystals as a seed stock microcrystals could be obtained, and after optimizing the concentrations of protein and precipitant they could be reliably produced

in a size of 15-20 µm and were consequently used for the time resolved experiment presented in **Paper III**. Repeating the seeding with crushed microcrystals led to more homogeneous growth and further increased the resolution of the crystals giving the 2.4 Å structure presented in **Paper I**.

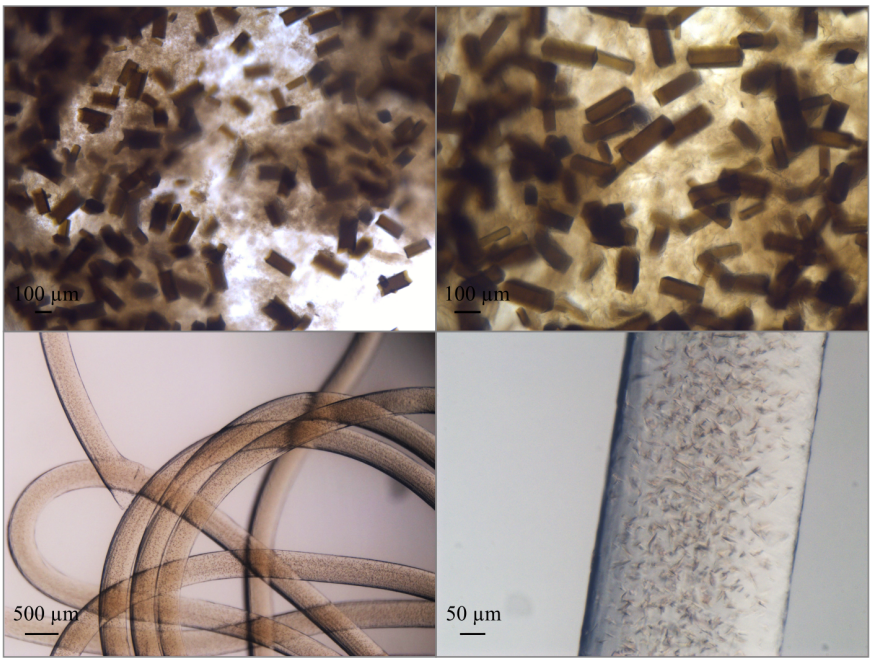


**Figure 4.1:** Examples of crystals. Top left: Large crystals of $RC_{Vir}$ grown at room temperature. Top Right: Large crystals of $RC_{Vir}$ grown at 4 °C and used as the base of the seed stock. Bottom left and right: LCP crystals of cytochrome c oxidase setup in 800 µl deep well plates.

## 4.2 Deep-well based LCP crystallization (Paper IV & Paper V)

When first used for crystallizing membrane proteins the LCP was prepared in Eppendorf tubes.[53] To create the sample volumes needed for SFX experiments this method has been developed into mixing the components in gas-tight syringes. This has now become the standard for LCP crystallization: After mixing the protein with monoolein a specific volume of the resulting lipidic phase is injected into a syringe of larger volume containing the precipitant through a syringe coupler. The coupler is then removed and the syringe is sealed. Following the growth of crystals the precipitant solution is ejected and the LCP can be collected by moving it to a different syringe. This way LCP from different syringes can be pooled and larger amounts can be prepared. Optionally, a thin steel wire can be inserted together with the LCP. This wire then creates a hook that can be used to pull out the LCP string from the precipitant after crystals have formed. This is the standard method of producing crystals of bacteriorhodopsin (**Paper VI**, **VII**, **VIII** and **IX**) and has been used successfully to give crystal structures with a resolution of 1.5 Å.

**Paper IV** and **V** present a new method of setting up LCP for SFX experiments using deep-well plates covered with a plastic film. Collecting the LCP is done by picking it out of the well with a Teflon-tip syringe piston, then packing it into gas-tight syringes for transport. The main difference compared to setting up in syringes is that this setup has an air gap that can have a huge effect on the crystallization process. An example of this can be seen in **Paper II** (figure 6.1), similar conditions produced rod-shaped nanometre-sized crystals in syringes and hexagonal-shaped microcrystals in deep-well plates. Setting up in plates has some advantages compared to setting up in syringes. One major reason is that it is much easier to monitor the crystallization process: a plate is better suited to use with a standard light-microscope. It is also easier to extract some LCP and put between glass slides by removing the cover film and replace it again. Another advantage is that there are more options for screening different conditions in the same plate whereas in syringes you would need one syringe for each condition. It is also possible to screen the diameter of the LCP and the rate at which the precipitant solution penetrates it by using needles of different diameters when setting up the plate. (Commercial syringe couplers only come in the "standard" size of ~400 µm inner diameter unless there is a possibility of constructing in-house couplers.)

Cytochrome c oxidase from *Thermus thermophilus* is a membrane-bound protein that catalyzes the reaction of converting molecular oxygen to water. Developing the protocol of setting up in plates led to the structure of this protein being

solved to 2.3 Å resolution at SACLA, Japan. In order to study its mechanism however, it needs to be handled in an oxygen-free environment. The method of setting up in plates has therefore been adapted to glass vials which can be purged with $N_2$ gas to crystallize both the reduced as well as the CO-bound form of the protein. Both the vials and the deep-well plates made it possible to scale up the volume of the crystallization with the prospect to produce several hundred microlitres of LCP at a time. For SFX experiments demanding millilitres of sample this makes sample production much less laborious.

The two methods presented here, seeding with a stock of microcrystals and crystallizing LCP in deep-well plates, ultimately gave the crystal form for solving the $RC_{Vir}$ structure presented in **Paper II**. (The vapour diffusion microcrystals were first tested with a mineral grease carrier media, but it was not compatible with the high ammonium sulphate content of the crystallization conditions.) One advantage of seeding in LCP for $RC_{Vir}$ is that the crystals are more homodispersely distributed within the LCP, whereas most other LCP crystals tend to grow more concentrated at the core of the LCP string (figure 6.1). This gives crystals more homogeneous in size and the risk of breaking them by extensively homogenizing the sample through a syringe coupler is reduced. The success of this crystallization method shows that seeding is viable for generating SFX microcrystals both in vapour diffusion and LCP setups.

# Chapter 5

# Paper I

In standard synchrotron focused crystallography it is common to aim for a large crystal as the increase in size usually leads to better diffraction and more resistance towards radiation damage. The consequence of this is that many strategies exist for producing single large crystals but much less is known about how to produce thousands of microcrystals needed for SFX experiments. With several synchrotrons installing the necessary equipment to do serial crystallography at microfocus beamlines as well as the possibility to do electron microscopy on micrometer-size crystals[116] the opportunities to get structural data from small well-diffracting crystals are greater than ever. In this paper a method to produce homogeneous microcrystals for SFX experiments from known vapour diffusion conditions is presented as well as a protein structure determined from these crystals.

## 5.1 Crystallization

The crystals were set up on-site at the LCLS in 20 µl sitting well drops mixing equal amounts of 10 mg/ml protein solution with a precipitant solution containing 1.8 M ammonium sulphate and 200 mM H123T against a 1 ml reservoir of 1.5 M ammonium sulphate. After 72 h 1 ml was collected into a 1.5 ml Eppendorf tube. These aliquots were vortexed with two seed beads (Molecular Dimensions) in 5-10 min rounds to mechanically break them apart, with resting on ice in between to prevent the sample from overheating. After each round of vortexing the sample was examined under a light microscope until visible crystal shards over 20 µm could no longer be observed. The sample was then concentrated by a factor of three by low-speed centrifugation (1000 x g) and removal of some of the mother liquor. The concentrated samples were then filtered through a 20 µm steel filter (VICI AG International) before loading it into the sample holder for the GVDN injection system. Due to the mechanical beating of the crystals by the beads there is some damage from this visible in the diffraction patterns as spot streaking. The crystal slurry itself is a heterogeneous mixture where the largest crystals in general gave better

diffraction than the smaller ones. The best way to get a higher amount of larger crystals is to vortex the sample for a shorter amount of time, but then the hit rate will also be lower as fewer smaller crystals will form and more pieces will get stuck in the filter. Nevertheless, this simple method of crushing crystals is an easy way to screen different crystal forms before optimising crystallization conditions for SFX and the structure of $RC_{Vir}$ could be solved to 3.3 Å. The crystal belonged to space group $P4_32_12$, a space group that several other high resolution structures of $RC_{Vir}$ belong to.[117–119]

Instead of mechanically crushing the crystals the next step was to optimise the conditions to produce microcrystals in order to get a more homogeneous sample for future experiments. The crushed crystals were vortexed until no visible crystal pieces could be detected when observed under a light microscope and used as a seed stock for new crystallization setups. It should be noted that this seed stock is used at a much higher concentration than in other seeding experiments as many nucleation sites are desired to produce a shower of microcrystals. In a "normal" crystallization setup aiming for macrocrystals, seeds are instead streaked into a new drop in order to have a few nucleation sites that larger crystals can grow from over a longer period of time. Optimizing these conditions by lowering the protein and precipitant concentrations gave microcrystals roughly 15-20 µm in size after three days of growth at 4 °C which now diffracted to 2.8 Å. The main reasons for this improvement in diffraction quality can be attributed to the removal of the vortexing step, which damaged the crystals, and growing them at a lower temperature to ensure that they do not form too rapidly. The concentrations of the protein and precipitant solutions seem to have a larger impact on crystal growth and size compared to the dilution of the seeds, but this most likely indicates that the seed stock is extremely concentrated from the start. Another improvement of the microcrystals compared to the crushed crystals is the homogeneity of the sample, as the crystals are more monodisperse in size there were fewer low-resolution patterns. This homogeneity was also seen for crystals of PSII when a similar microseeding protocol was employed.[120]

In addition to the microcrystals already produced, a second round of seeding was tested where the microcrystals were crushed by the same manner and used as seed stock in the same crystallization conditions. The microcrystals were more difficult to break compared to the large crystals and when visually inspected they appeared as if they retain a more crystalline shape in the seed stock. Crystals growing from this second round of seeding were even more homogeneous in size and diffracted to 2.4 Å.

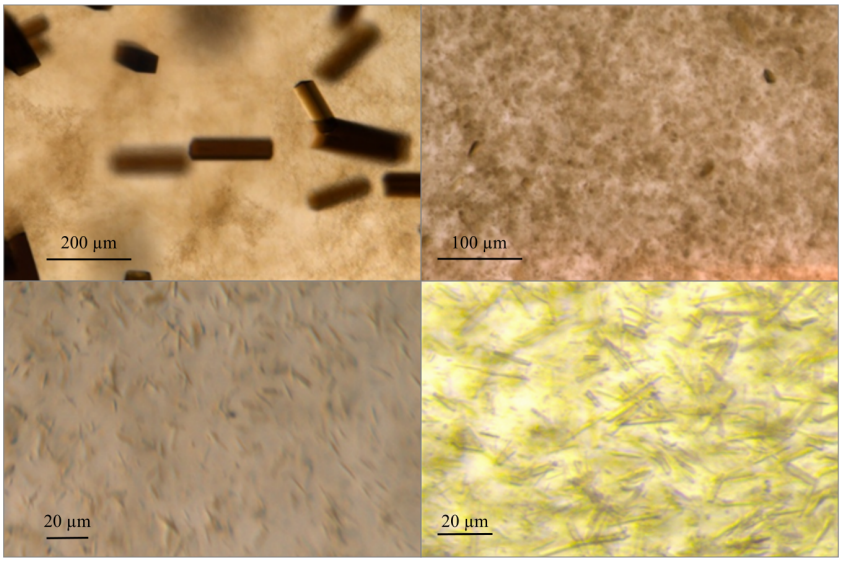


**Figure 5.1:** Different crystal forms used in the experiment. Top left: Large crystals grown at room temperature. Top Right: Seed stock prepared from crystals grown at 4 °C. Bottom left: Microcrystals after one round of seeding. Bottom right: Microcrystals after two rounds of seeding.

## 5.2 Data collection and refinement

Diffraction data was collected at the Coherent X-ray Imaging (CXI) beamline at the LCLS during three experiments in 2014, 2015 and 2016. (Detailed experimental parameters can be found in the method section of **Paper I**.) Crystals were set up on site either without seeds or a with a seed stock made from microcrystals that was brought from Gothenburg to achieve the one or two rounds of seeding. The crystals were collected after 72 h and concentrated and filtered as described above then loaded into the GVDN system on a cooled rocking table[121] to prevent settling of the crystals in the sample reservoir. The crystals were injected into the X-ray beam through a 75 µm diameter nozzle with the X-ray sampling the crystals at a 120 Hz repetition rate. The data was recorded on a Cornell–SLAC Pixel Array Detector (CSPAD)[98, 122] and diffraction hits were sorted from the empty frames by Cheetah.[123] The detector geometry was optimized with geoptimizer[124] in CrystFEL[125] v. 0.6.2 and the collected images were indexed using Mosflm[62, 63] and Dirax[126] in space group $P4_32_12$ for all three crystal forms. The indexed patterns were

merged and scaled with the partialator module in CrystFEL. The merged intensities were converted to structure factors using the CCP4[94] module Truncate[127] and molecular replacement was done with the CCP4 module Phaser[93] using a 1.96 Å structure (PDB code 2I5N[117]) as search model yielding one solution. The structure was improved by 20 cycles of rigid body refinement in the CCP4 module Refmac[128] followed by several rounds of restrained refinement and manual model building in Coot.[129]

## 5.3 Structure

Over the years multiple structures of $RC_{Vir}$ have been submitted to the Protein Data Bank (PDB). Compared to our SFX LSP structures the double-seeded structure from 2016 with a resolution of 2.4 Å shows structural features at a much higher detail. One of the major results from this data is that even though the resolution is not as high as structural data collected for some crystals at synchrotrons, the large number of images collected leads to a higher multiplicity and the visualization of new structural features. The most prominent effect of this is seen in a flexible loop region in the H-subunit between $Glu45_H$ and $Pro54_H$ which in previous structures has not been modelled. In the SFX data, if the loop is omitted there is a clear feature for this in the $F_{obs}$-$F_{calc}$ map when contoured at 3.0 $\sigma$. After building in the missing residues there is a continuous density in the $2F_{obs}$-$F_{calc}$ map of that region (figure 5.2). It should be noted that recently a Cryo-EM structure of $RC_{Vir}$ in complex with LH1 has been published[8] which puts the loop in a different conformation. In that structure the loop is constrained by one of the LH1 proteins surrounding the RC while in the SFX structure the loop is aligned against the closest molecule in the crystal structure which to some extent stabilizes it. While not being the the same conformation of the loop as that for the RC-LH complex the SFX structure nevertheless shows the full structure of the crystallized protein. As most structural investigations are performed with single proteins it is a powerful tool to be able to visualize the flexible regions.

Superposing the structure with lipids from synchrotron data in the same space group reveals two new lipid binding sites. Both of these sites are located in the membrane region of the side of the protein that has a deeper groove and therefore represent a region of high flexibility. Rather than fitting into pockets, these lipids sit on the surface of the protein. Contrary to this, a lipid found in previous structures situated in a pocket along the M-branch could not be modelled into the electron density with any certainty. By comparing the internal $C_\alpha$ distances of structures it is possible to sort them based on structural similarity. This was performed for all $RC_{Vir}$ structures published to date and shown as a tree diagram in figure 5.3.

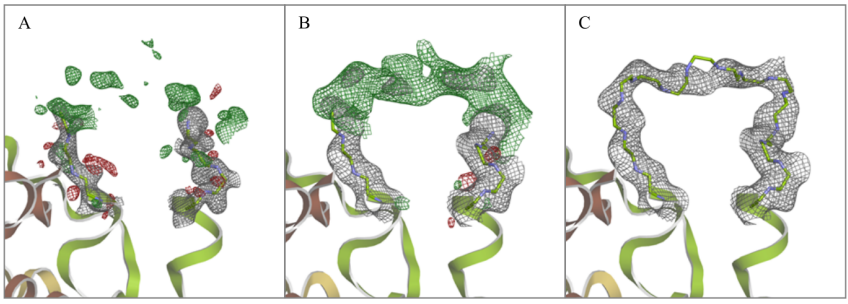


**Figure 5.2:** $2F_{obs}$-$F_{calc}$ and $F_{obs}$-$F_{calc}$ of the loop region in the H-subunit between residues 45-54 contoured at 1.0 $\sigma$ (grey) and 3.0 $\sigma$ (green and red) respectively. A: Density of 2I5N, the model used for molecular replacement. B: Density before building the model. C: Density after building the main chain of this region.

Unsurprisingly, all three SFX structures cluster together with each other as they have very similar unit cell parameters. They also sort closely to other structures of the same space group, showing that this factor is more important for structural similarity than temperature or acquisition mode.

## 5.4 Discussion

For a long period most crystallization strategies have focused on producing the large well diffracting crystals needed for structural determination at synchrotrons. In this process microcrystals are often seen as a good crystal lead for a potential macrocrystal but, due to their sensitivity to radiation damage, not that many strategies exist to produce them. Both the crushing of large crystals and seeding from known conditions represent two relatively easy ways to achieve the sample necessary for XFEL experiments. Especially the method of crushing the crystals, while crude, is an easy alternative to screen different batches of crystals without spending the extra effort of finding the perfect conditions for microcrystals of the correct size. Provided that the crystallization conditions are not too harsh the crystals can also be mixed with grease and used with a viscous injector decreasing the amount of sample needed considerably. By seeding the resolution of the crystals improved from 3.3 Å to 2.4 Å which is a significant increase in the type of information you can gain in a time resolved experiment. Seeding could potentially also be used in conditions that already produce microcrystals to improve homogeneity as these types

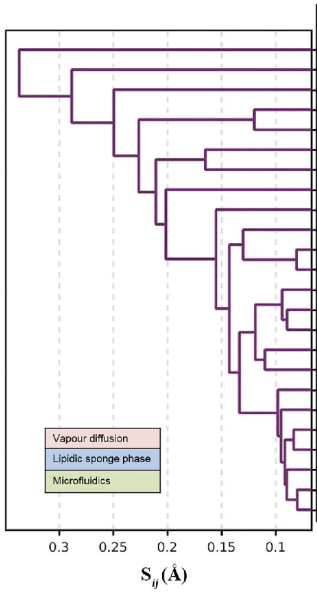


| PDB ID | Year | Res (Å) | Collaboration | Xray Source | Temp (K) | Space Group |
|---|---|---|---|---|---|---|
| 1R2C | 2003 | 2.86 | Norris | Synchotron | 293 | P 43 21 2 |
| 4CAS | 2013 | 3.50 | Neutze | XFEL | 293 | P 21 21 21 |
| 4AC5 | 2011 | 8.20 | Neutze | XFEL | 263 | P 21 21 21 |
| 2X5V | 2010 | 3.00 | Neutze | Synchotron | 293 | P 21 21 2 |
| 2X5U | 2010 | 3.00 | Neutze | Synchotron | 293 | P 21 21 2 |
| 2WJN | 2009 | 1.86 | Neutze | Synchotron | 100 | P 21 21 2 |
| 2WJM | 2009 | 1.95 | Neutze | Synchotron | 100 | P 21 21 2 |
| 3D38 | 2008 | 3.21 | Ismagilov | Synchotron | 100 | P 31 2 1 |
| 1PRC | 1988 | 2.30 | Michel | Rot. Anode | 271 | P 43 21 2 |
| **5O64** | 2014 | 3.30 | Neutze | XFEL | 293 | P 43 21 2 |
| **5O4C** | 2015 | 2.80 | Neutze | XFEL | 293 | P 43 21 2 |
| **5NJ4** | 2016 | 2.40 | Neutze | XFEL | 293 | P 43 21 2 |
| 3T6D | 2011 | 1.95 | Cogdell | Synchotron | 100 | P 43 21 2 |
| 3T6E | 2011 | 1.92 | Cogdell | Synchotron | 100 | P 43 21 2 |
| 2I5N | 2006 | 1.96 | Ismagilov | Synchotron | 100 | P 43 21 2 |
| 3G7F | 2009 | 2.50 | Norris | Synchotron | 100 | P 43 21 2 |
| 1VRN | 2005 | 2.20 | Norris | Synchotron | 100 | P 43 21 2 |
| 2PRC | 1997 | 2.45 | Michel | Synchotron | 263 | P 43 21 2 |
| 2JBL | 2006 | 2.40 | Ditchfield | Synchotron | 263 | P 43 21 2 |
| 3PRC | 1997 | 2.40 | Michel | Synchotron | 263 | P 43 21 2 |
| 1DXR | 2000 | 2.00 | Michel | Synchotron | 263 | P 43 21 2 |
| 7PRC | 1997 | 2.65 | Michel | Synchotron | 263 | P 43 21 2 |
| 6PRC | 1997 | 2.30 | Michel | Synchotron | 263 | P 43 21 2 |
| 5PRC | 1997 | 2.35 | Michel. | Synchotron | 263 | P 43 21 2 |

**Figure 5.3:** Comparison of $C_\alpha$ distances between deposited structures of $RC_{Vir}$. The three structures from this paper are marked in bold as 5O64 (2014), 5O4C (2015) and 5NJ4 (2016).

of microcrystals are often the result of fast growing crystals in high precipitant concentrations. Furthermore, fine-tuning the concentrations of protein and precipitant, as well as the dilution of the seeds allow the manipulation of growing crystals to a specific size.[130]

The 2.4 Å structure that is the result of this work is a slightly lower resolution than the highest resolution synchrotron structures of $RC_{Vir}$. However, because of the multiplicity stemming from the XFEL data collection it is still on par with these structures in the quality of the data, especially considering that there is density for the backbone of the loop in the H-subunit which is often poorly defined. With SFX there is also the advantage of collecting data at room temperature without the radiation damage of sensitive features such as metals.

## 5.5 Summary of Paper I

In this paper a method for generating microcrystals for SFX experiments is presented based on crushing macrocrystals until the correct size is achieved. A second method involving seeding is also presented, which achieves the proper nucleation conditions for the growth of homogeneous microcrystals. Through application of these methods the resolution of $RC_{Vir}$ could be improved from 3.3 to 2.4 Å and the method of generating crystals from seeding is at the core of the work done in **Paper III**. In the 2.4 Å structure there are two more lipids compared to synchrotron structures, there is also visible occupancy for a flexible loop in the H-subunit. These new features are likely due to the high multiplicity of the data.

# Chapter 6

# Paper II

A key limitation of the crystals grown in vapour diffusion is the low occupancy of the $Q_B$ pocket. This arises because of the natural mobility of the $Q_B$ and the presence of detergent in the buffers, meaning that some of the native UQ will go into solution during protein purification and crystallization.[131] In order to pursue time resolved experiments examining longer time points including two-flash studies, it is imperative that the $Q_B$ pocket has full occupancy to get a strong enough signal in a difference map. One of the main advantages of LCP is the possibility to add both hydrophilic and hydrophobic compounds to the crystallization setup, so while the UQ is mostly insoluble in the protein buffer it can easily be mixed with the monoolein. In addition, an LCP crystal form can also take advantage of the slower flow of the viscous injector.

## 6.1 Crystallization

The first crystallization screens were set up with a robot using monoolein doped with ubiquinone-2 (UQ2). The hits were all either in conditions similar to previously reported ones based on H123T, or from the commercial screens containing other diols such as butane-1,4-diol and hexane-1,2-diol. One condition in particular looked interesting as it had triangular crystals in it, compared to the rod-shaped crystals previously obtained, and this was used as the base conditions for scaling up (figure 6.1). The first large scale crystal batches were set up in syringes, which is the most popular way of growing crystals in LCP. For $RC_{Vir}$ this condition yielded small needle-shaped crystals that diffracted to 2.4 Å when tested at SACLA. However, the hit rate of these crystals were not satisfactory and it was deemed that very few of them diffracted due to their limited size.

Returning to screening, the plate method developed in **Paper IV** was included in the trials, beginning by setting up in Eppendorf tubes to mimic this on a smaller scale. Using this method the crystals from the initial screening returned, this time

as hexagonally shaped crystals that polarize light (a feature not seen for the vapour diffusion crystals). A second condition was also found by mixing the protein solution with the same seed stock as in **Paper I** before preparing the LCP, then setting up in plates containing precipitant solutions with lower salt concentrations. When testing the two new crystal forms at SACLA they both gave satisfactory diffraction and hit rate. The hexagonal crystals diffracted to 2.2 Å. Unfortunately, the crystals had a very long c-axis in the unit cell and the images from this crystal form could not be indexed. (The data indicates that these crystals belong to a space group with hexagonal symmetry so they are different from the previous LSP crystals belonging to $P2_12_12_1$.) The seeded crystals diffracted to 2.3 Å and the structure could be solved at 2.4 Å resolution with the number of images collected.

Removing the seeds from the second crystallization condition stops any visible crystals from forming, they are therefore clearly needed for the nucleation in the crystallization process. The crystals have the space group $P2_12_12$ which is different from the seeds belonging to $P4_32_12$. The crystals must therefore either grow from the seeds using them as initial building blocks but then conforming to the surrounding conditions, or they are the result of melted seeds that produce thousands of spots of highly concentrated protein. Either way, the seeding produces crystals that are much more homodisperse both in size and location inside the LCP string. It is also possible to fine-tune the crystal size and density by slightly altering the ratio between protein and monoolein during mixing where a higher protein content gives crystals that are fewer but larger, and a higher monoolein content gives crystals that are smaller and denser. For a 75 µm injector nozzle crystals should not be larger than approximately 30 µm. By mixing in the optimized ratios, 20-25 µm sized crystals can be produced having a hit-rate of up to 30 %. (Note that statistically the optimal hit rate is approximately 60 %, as higher hit rates gives more images containing multiple patterns.[132])

## 6.2 Data collection at SACLA and refinement

Crystals were prepared in Gothenburg two weeks prior to the experiment and packed in 500 µl gas-tight syringes (Hamilton) for storage and transport. Data was collected at the BL-2 beamline at SACLA, Japan in February 2018. The sample was homogenized by pushing it back and forth a few times between two 100 µl syringes connected through a syringe coupler. It was then injected into a sample cartridge using a needle and subsequently loaded into an injector mounted with a 75 µm nozzle. The sample was injected into the X-ray beam at 1 µl/min using a 7.5 keV beam operated at 30 Hz and a multi-port charge-coupled device (MPCCD) detector[99] with a distance of 50 mm. Diffraction hits were sorted from empty frames

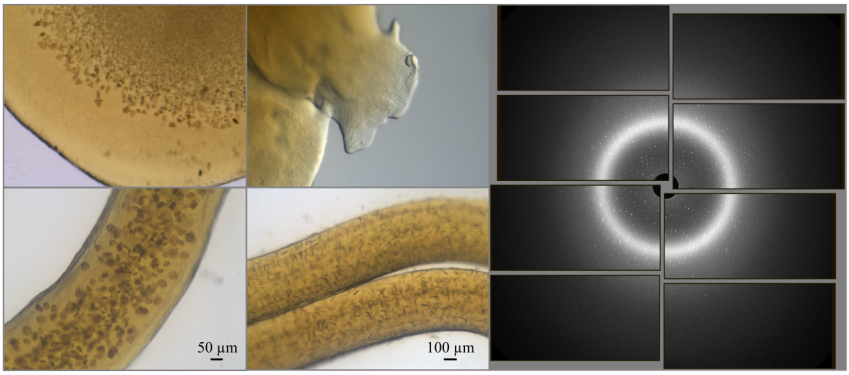


**Figure 6.1:** Top left: Screening conditions giving triangular crystals used as base conditions for scaling up. Top middle: Nanocrystals from setting up in syringes. Bottom left: Hexagonal crystals from plates. Bottom middle: Seeded crystals from setting up in plates ultimately used for determining the structure. Right: Diffraction pattern from the seeded crystals, the edge of the detector is ~2.2 Å.

using Cheetah[123] and images were indexed with CrystFEL[125] v. 0.6.3 using the peakfinding algorithm from Cheetah and DirAX[126] as the indexing method. 5912 patterns could be indexed from 7488 images giving an indexing rate of 79 % and a total indexing rate of 2.8 % for all images including non-hits. Merging and scaling was done with orthorhombic symmetry in CrystFEL using the partialator module. The intensities were converted to structure factors using Truncate[127] in CCP4[94] and molecular replacement was done with Phaser[93] using a 1.96 Å structure (PDB code 2I5N[117]) as search model. The structure was run through 20 cycles of rigid body refinement in Refmac[128] followed by multiple rounds of restrained refinement and manual building in Coot.[129]

## 6.3 Structure

The main reason for switching to LCP was to get occupancy for the mobile ubiquinone, since large concentrations of UQ2 or UQ1 can be mixed into the monoolein. In the refined structure the ring of the quinone is defined but the density for the tail only covers the first isoprenoid unit. An omit map (the structure refined with an empty $Q_B$ pocket) shows clear density for the ubiquinone confirming that it is present (figure 6.3). There are two possible positions that the ligand can adopt in the pocket referred to as the proximal and distal positions. These were first

shown in the reaction center from $RC_{Sph}$, and it was proposed that the movement between these two positions could be initiated by photon absorption and thereby act as a gating mechanism for electron transfer since the reduction of the quinone will only take place in the proximal position.[32] The original $RC_{Vir}$ electron density data was then remodelled with the UQ mainly in the distal position seemingly confirming this theory.[35,133] However, the distribution between the two sites appear to depend on many factors which also include detergent choice and crystallization conditions.[134] FTIR studies have shown that the movement of $Q_B$ upon illumination is absent[33] and additional freeze-trapping of light and dark crystals of $RC_{Vir}$ also showed predominantly proximal binding.[34] In this structure the ubiquinone is mainly in the proximal position closer to the non-haem iron, but the B-factors of the ligand are slightly higher (~70) compared to the surrounding amino acids of the protein (~50) indicating some mobility. This is consistent with other reported structures of $RC_{Vir}$.[34,117]

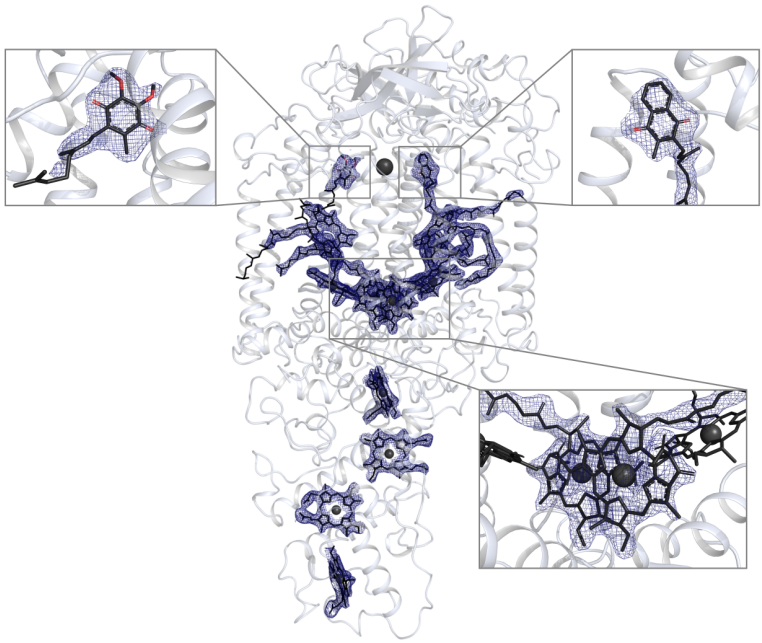

**Figure 6.2:** The structure coordinates of the model from the seeded crystals with the density of cofactors contoured at 1.0 $\sigma$.

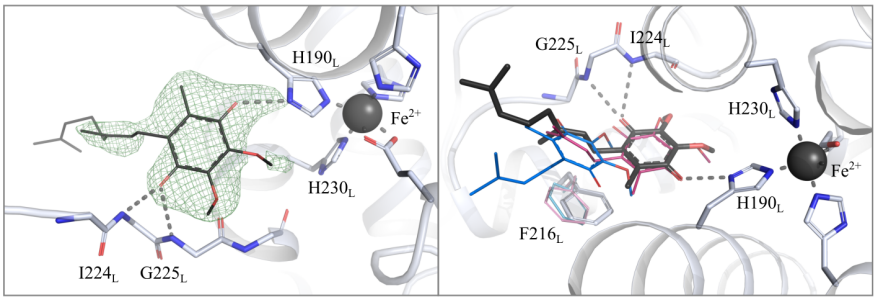


**Figure 6.3:** Left: $F_{calc}$-$F_{obs}$ map of the $Q_B$ site contoured at 3.0 $\sigma$ generated by refining the structure in Refmac with the ligand removed. (UQ2 is included in the figure as reference). Right: Overlay with $RC_{Sph}$[32] showing proximal (pink) and distal (blue) positions.

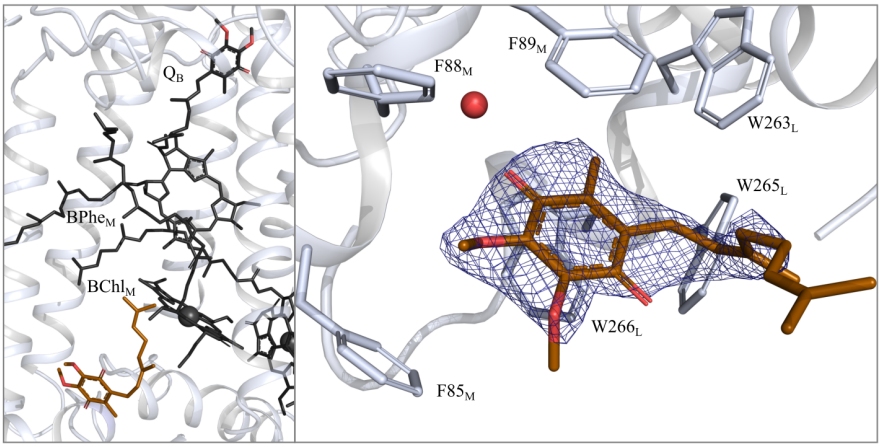


**Figure 6.4:** Second UQ2 site. Left: Its position in relation to the other cofactors as in figure 6.2. Right: Density contoured at 1.0 $\sigma$.

In the structure there is also a second UQ2 site close to the $BChl_M$ where it fits into a pocket surrounded by phenylalanines (figure 6.4). This is consistent with other crystal structures of $RC_{Vir}$ and not surprising considering the excess of UQ2 in the crystallization conditions. Apart from this there are relatively few lipids in the LCP structure, especially compared to the microcrystal structure in **Paper I**. Due to being in a different space group one of the lipids that is consistent across many $RC_{Vir}$ structures is absent because of crystal contacts. It is also possible that the lipids have a higher mobility in the lipidic phase of the crystallization conditions and are therefore more difficult to model as a result. One LDAO molecule in

the microcrystal structure has been exchanged for a monoolein showing that the detergent micelle at least in part has been dissolved.

## 6.4 Discussion

While XFEL beamtime is difficult to access to most users, microcrystals nowadays have a much larger potential to be useful as the equipment to perform SFX is installed at more synchrotrons around the world. It might be considered by some that the synchrotron setups are nothing more than screening for XFEL beamtime but the structural data generated at synchrotrons can still be of the same quality as that of an XFEL with only a minor reduction in resolution.[135]

Seeding is a common technique in liquid crystallography, but not that much has been previously reported in LCP experiments. If the crystallization conditions for crystals grown by vapour diffusion or batch makes them incompatible for mixing with grease, this method could be a possible short-cut on the path towards finding conditions in the lipidic phase. It is also possible that seeding in this way might generate crystals in conditions where non-seeded protein would draw a blank. LCP is often used to crystallize membrane proteins, but they are sometimes notoriously difficult to grow to a larger size due to the lower concentration of protein solution in the cubic phase.[136] One method of screening for new conditions in LCP is to collect the phase containing smaller crystals and dispense it into new screening conditions hoping the crystals will act as seeds for growing macrocrystals.[137] Hypothetically, one could then make microcrystals by the same method simply by adding these to a new syringe after making the LCP phase. A further option would be to break the crystals first either mechanically or by running the mix back and forth through a syringe coupler a few times to increase the microseed concentration.

Just as for the microcrystals generated in **Paper I**, a homogeneous crystal sample could be generated by adding a seed stock to the protein solution in the crystallization setup. Having this crystal form in LCP with occupancy for the mobile ubiquinone in a position allowing electron transfer opens up new possibilities for time resolved experiments of longer time points and two-flash studies as well as data collection at synchrotrons. Optimizing the density of the crystals has the potential to increase the hit rate 5-fold compared to the vapour diffusion crystals, which would lower the sample consumption and data collection times considerably.

## 6.5 Summary of Paper II

A protocol for generating microcrystals of $RC_{Vir}$ in LCP by seeding with crushed vapour diffusion crystals has been developed and an initial dataset from this crystal form was collected at 2.4 Å resolution. UQ2 was doped into the monoolein used in the crystallization setup with the result that the mobile quinone in the structure has density comparable to the other cofactors in the protein. These crystals are promising for future experiments as they have good resolution and much higher hit rates than previous crystal forms.

# Chapter 7

# Paper III

In the first 200 ps following the initial absorption of a photon the electron from the P960 has already crossed the transmembrane region and reached the MQ (menaquinone-9) in the $Q_A$ position. Including the $BChl_L$, this covers a distance of approximately 20 Å which is comparable to the theoretical transfer rate suggested by Marcus.[25,37] The first two transfer steps in this process to the $BPhe_L$ extend roughly half of that distance in ~3 ps (figure 7.1). Much work has been done on the kinetics of the initial charge-separation and whether or not the tunnelling to the $BPhe_L$ is a one- or two-step process that involves the secondary $BChl_L$. There is however, some spectroscopic evidence that this charge separation is more than a simple electron transfer where the electron makes the jump once the energy barrier can be crossed and that ultrafast movements in the protein are also involved in this process.[40] Unveiling these movements would be of great use for understanding electron transfer processes in photosynthesis as well as other biological assemblies. As the initial photoexcitation of the P960 takes place in femtoseconds the use of XFEL radiation is a suitable medium to study these potential changes in the structure. The aim of the experiment in this paper was to irradiate microcrystals with a 960 nm laser to capture changes in the protein after 5 and 300 ps in a pump-probe manner, the experiment was then repeated one year later also including 1 ps as a time point.

## 7.1 Crystallization and data collection

Crystals were grown with one round of seeding as described in **Paper I** at the CXI beamline at the LCLS in April, 2015. The crystals were collected after 3 days of growth, concentrated 3 times by centrifugation (1 min at 1000 g) and removal of the mother liquor. They were then filtered through a 20 μm stainless steel filter (VICI AG International) to avoid clogging the GVDN injector system. The sample was loaded into reservoirs and placed on the sample rocker[121] to keep the crystals from settling during injection. The sample was injected into the vacuum chamber

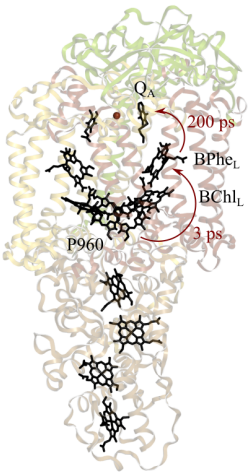


**Figure 7.1:** Reference structure showing the electron transfer steps relevant for this paper.

of the beamline at 25 µl/min. The X-rays were operated at 120 Hz with an energy of 6.6 keV, a pulse length of 36 fs and a 10 $\mu m^2$ spot size. To induce electron transfer in the protein a Ti:Sa laser was aligned with the sample operating at 960 nm to directly excite P960 with a 150 fs pulse length, 11.75 µJ pulse energy and a 190 µm full width at half maximum spot size. The laser was controlled with the timing tool of the beamline[101] and run at 120 Hz matching the repetition rate of the XFEL. Data was collected at 5 and 300 ps in addition to the ground state for which data was collected without photoactivation. Diffraction hits were collected on the CSPAD[98,122] with a detector distance of 89 mm, sorted from dark images by Cheetah[123] and indexed with CrystFEL[125] v. 0.6.2 using Mosflm[62,63] and DirAX[126] after optimizing the geometry with geoptimizer.[124] The data was then scaled and merged in the partialator module of CrystFEL. The experimental details for the 1 ps time point can be found in the methods section of **Paper III**.

## 7.2 Calculation of density, difference density and partial occupancy maps.

The structure for the dark images was refined to give the atom coordinates of the ground state. This was done in CCP4[94] by converting the intensities to structure factors with the Truncate[127] module, followed by molecular replacement in the

Phaser[93] module using the 2.4 Å microcrystal structure from **Paper I** (PDB code 5NJ4) as search model. The solution was refined in Refmac[128] by 20 cycles of rigid body refinement followed by several cycles of restrained refinement and manual building in Coot.[129] Isomorphous difference density maps for the 5 and 300 ps time points were calculated with the phases from the refined dark state structure. The 1 ps time point was similarly calculated against the dark data from the 2016 experiment. The maps were further refined by a Bayesian weighting[104] to improve the signal to noise ratio. For the areas of the protein where significant movement could be seen an alternative conformation was added at 30 % occupancy (mainly around the $Q_A$ site and the helices extending to P960). This was then run through 10 cycles of refinement in Phenix.refine[95] against the light data while only letting the alternative conformations move to generate excited state atom coordinates.

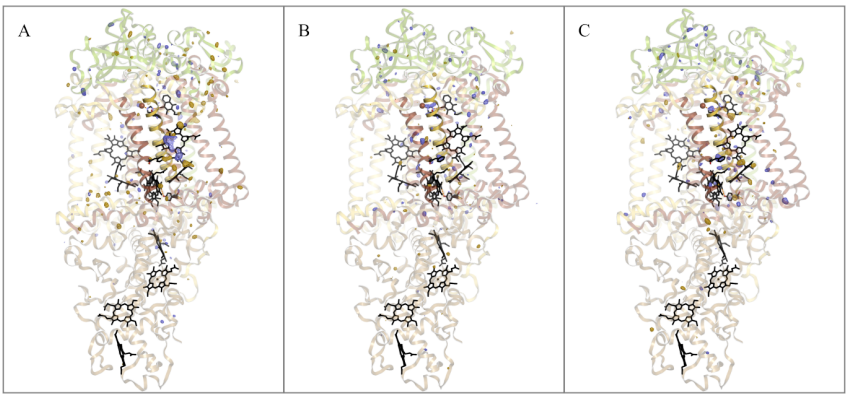


**Figure 7.2:** Difference density maps for the three time points contoured at 4.0 $\sigma$. A: 1 ps. B: 5 ps. C: 300 ps.

## 7.3 Changes in structure

Looking at the overall movements of the protein in the difference density maps it can be seen that they are mainly concentrated around the central cofactors taking part in the studied electron transfer steps (figure 7.2). These include the P960, $BChl_L$, $BPhe_L$ and MQ as well as the helices connecting the P960 to the two quinone binding sites. For the special pair the two chlorophyll cofactors move closer together, a movement that develops over the three time points measured.

It is at the strongest at 300 ps, where a neighbouring tyrosine ($Tyr195_M$) is moving together with the acetyl substituent of the chlorophyll (figure 7.3). However, the same movement cannot be seen for the symmetrically equivalent histidine $His168_L$.

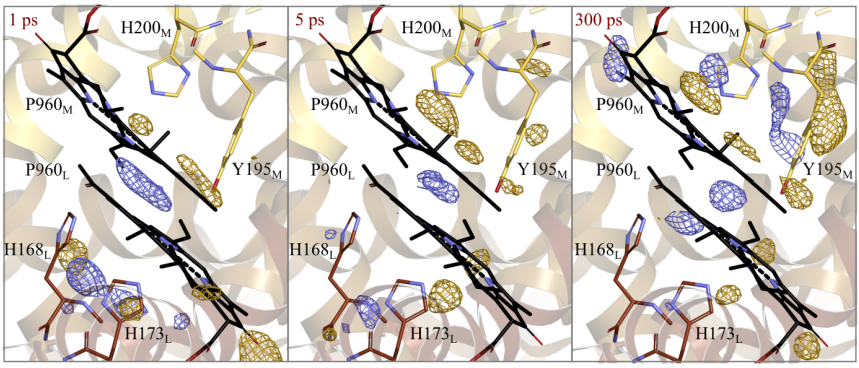


**Figure 7.3:** Difference density of P960 after 1, 5 and 300 ps contoured at 3.3 $\sigma$. Blue density represents positive features and yellow density represents negative features.

After 300 ps the electron has moved to the MQ in the $Q_A$ position. This is accompanied by a movement of the MQ closer to the non-haem iron as well as a shortening of the hydrogen bond to the coordinating histidine. In addition to the MQ itself, there is a strong movement of the $E_M$ and $D_M$ helices around this cofactor (figure 7.4). As expected there is very little movement of the MQ after 1 or 5 ps, but in the 5 ps map there is already a slight movement of the same helices.

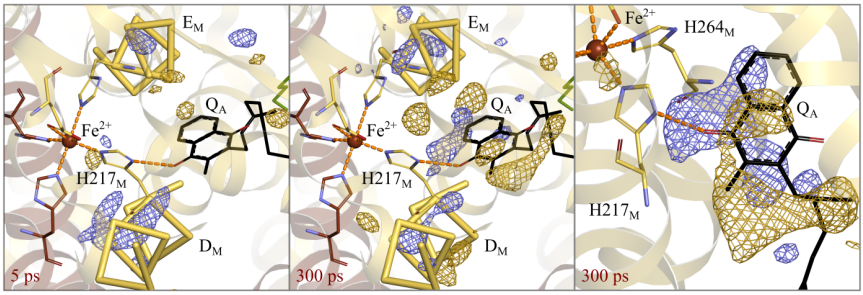


**Figure 7.4:** Difference density around the MQ and surrounding helices after 5 and 300 ps. Overall view is contoured at 3.5 $\sigma$ and the closeup of the MQ is contoured at 3.0 $\sigma$.

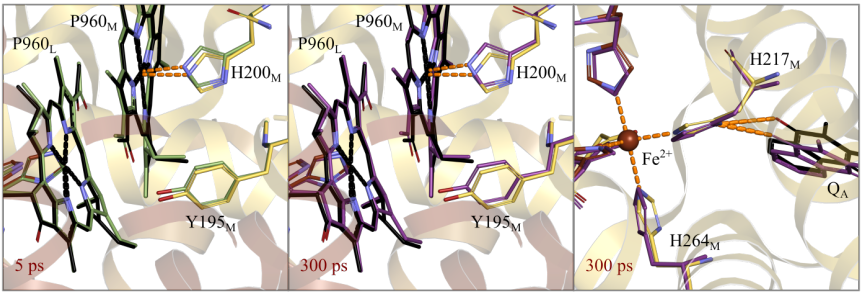


**Figure 7.5:** Calculated maps of the excited state structures at 5 and 300 ps.

The movement of these two sites can also be visualized in the calculated structures of the excited states (figure 7.5). The $Tyr195_M$ interacting with the P960 is moving closer to the carbonyl oxygen of the chlorophyll acetyl group by 0.2 Å as the acetyl group is moving closer to the second chlorophyll of the P960. Similarly the MQ is also moving closer to the non-haem iron by 0.25 Å.

## 7.4 Discussion

Both the 5 ps and 300 ps time points show the protein after electron transfer has taken place, with the P960 having a positive charge and the $BPhe_L$ or the MQ having a negative charge. This likely means that the larger structural movements shown are those of the protein responding to the change in charge distribution. This holds true for the larger movements of the P960 and the MQ seen for 300 ps. For P960 having the two chlorophylls moving closer would mean stabilizing the positive charge of these cofactors. What is interesting is that this movement can be seen already in the 1 ps map before charge separation has taken place. It might therefore imply that part of this movement is a response to the photon absorption itself and there are some energy redistributions taking place in the P960 in preparation for the electron transfer. However, as the excited state is formed within femtoseconds further studies on shorter time points would be needed to elucidate what is happening at this stage.

At the $Q_A$ site there is also a strong movement at 300 ps where the negatively charged MQ moves closer to the non-haem iron. This is accompanied by the movement of the surrounding helices. It should be noted that both the $Tyr195_M$ next to the P960 as well as the residues surrounding and moving together with the MQ belong to the same transmembrane helix of the M-subunit connecting the P960 with the MQ. The charge stabilization and movement of P960 could therefore have an

allosteric effect on the movements that later takes place around the quinones. A mutational study in PSII exchanging amino acid residues to bulkier ones in the D and E helices (the two helices closest to the centre of the protein) affected the electron transfer from $Q_A$ to $Q_B$,[138] indicating that the movement of these helices have an effect on the function of the protein. By the same reasoning that movements occur due to charge stabilization you would expect the $BPhe_L$ to show a large movement after 5 ps. However, this does not occur, possibly because it has a larger conjugated system compared to the MQ and can mitigate the negative charge better. It also interacts with the nearby $E_M$-helix (Extended Fig C and D, **Paper III**) but how much of an effect this represents is difficult to say.

One major challenge in interpreting SFX data is that you need clear difference density peaks (preferably above 3.5 $\sigma$) to determine a likely structural movement. This is to prevent over-interpretation of experimental results as difference density maps inherently contain much noise. The problem with putting this restriction on analysis is that small consistent structural movements important for the function of the protein may end up below this threshold. For this study, the movements of the P960 and the MQ are examples of definite movements that take place. However, it is possible that some of the weaker movements around the helices cannot be seen, and extracting this kind of information from the data in a convincing way will be very difficult. Fortunately, the multiplicity of SFX data is several orders of magnitude higher than that for synchrotrons. There is ongoing work to generate a multitude of structures from this data in order to cross-correlate them and produce common movements between them. Doubtless, additional methods of analysing SFX data will appear as the method becomes more widespread.

## 7.5 Summary of Paper III

The microcrystals developed in **Paper I** was used for a time-resolved experiment at the LCLS to photoexcite the P960 and investigate the structural changes after 1, 5 and 300 ps. Major structural changes can be seen after 300 ps involving the bacteriochlorophylls of P960 moving closer to each other and the MQ moving closer to the non-haem iron. There are also smaller movements in the helices surrounding these cofactors.

# Chapter 8

# Conclusions and Outlook

Using XFEL radiation to solve protein structures is more and more common, with this serial crystallography is becoming more common as well. This requires new methods of crystallizing to generate the microcrystals needed for these types of experiments.

In **Paper I** new methods to create microcrystals for XFEL experiments are presented. The simplest one of mechanically crushing macrocrystals can be used for crystals independent on the crystallization conditions and is a simple way to test for diffraction without spending numerous hours on optimizing crystallization conditions for microcrystals. We have also shown that it is possible to solve the structure from these crystals, but the amount of damage on the crystal integrity incurred by the crushing will vary and must be evaluated on a case by case basis. The main result of this paper is the seeding protocol developed by using our crushed crystals as nucleation sites for new microcrystals. In this way the crystal size of $RC_{Vir}$ could be reduced to a tenth of what it normally crystallizes to. By seeding a second round it was also possible to increase the resolution of the structure solved from these crystals. For time-resolved experiments that depend on having high resolution data this technique have the possibility to improve difference map data immensely.

Seeding was also used as a technique in **Paper II** to crystallize $RC_{Vir}$ in LCP and solve the structure with occupancy for the $Q_B$ site. The addition of seeds in this case led to microcrystals more homogeneously dispersed in the LCP compared to non-seeded conditions. The method of setting up LCP crystals plates was initially developed in **Paper IV** and **Paper V** for the crystallization of cytochrome c oxidase. Setting up in deep-well plates allows scaling up the volume of crystallization to easily produce the amounts needed for time resolved SFX experiments. It enables more options when screening for crystals and makes it easier to follow the crystallization progress. The method can be adapted to different types of vials and plates if additional sample preparation is needed for the experiment. Additionally,

there is the possibility to do samples oxygen-free or adding different compounds to the precipitant for soaking the crystals. Adapting the methods presented here will hopefully lead to more generalized ways of producing microcrystals.

In **Paper III** microcrystals of $RC_{Vir}$ were used to perform a time resolved experiment at an XFEL. By probing the crystals with a 960 nm laser it was possible to look at the structural movements 1, 5 and 300 ps after the initial photon absorption. There are definite movements around the P960 as well as the MQ and the surrounding helices. However, some of these structural movements can be seen already at 1 ps which is before the charge separated state has formed. An interesting aspect for future experiments would therefore be to investigate even shorter time points to figure out the extent at which the protein moves in response to photon absorption. The high occupancy of the $Q_B$ site in the LCP structure also opens up the possibility to do time resolved experiments on longer time scales, including a two-flash experiment to fully reduce the $Q_B$.

# Chapter 9

# Populärvetenskaplig sammanfattning

Proteiner är molekyler uppbyggda av aminosyror och är det atomära maskineriet i vitt skilda biologiska processer. Cellmembran är en form av fett-strukturer (även kallade lipid-strukturer), dessa bildar ett skikt mellan två vattenfaser och separerar dem enligt principen att olja och vatten ej blandar sig. Membranproteiner är en typ av proteiner som ofta befinner sig i cellmembranet, där utgör de kopplingen mellan insidan och utsidan av cellen genom att till exempel ta emot signaler från utsidan eller transportera molekyler och joner genom membranet. För att binda till membranet är ytan på dessa proteiner till viss del hydrofobisk, det vill säga de löser sig inte så lätt i vatten. Det gör att man måste ta till speciella metoder för att jobba med dem.

Ett sätt att undersöka den atomära strukturen på proteiner är att skapa proteinkristaller och skjuta på dem med röntgenstrålning. Kristallen reflekterar en del av röntgenljuset och med hjälp av dessa reflektioner kan man beräkna positionerna av atomerna i proteinet, det vill säga strukturen av proteinet. När man vet hur proteinet ser ut kan man använda den informationen för att förklara hur det fungerar. För proteiner som går att aktivera kan man även titta på skillnaden i strukturen mellan två olika tidpunkter för att se hur atomerna förflyttas. En ny typ av röntgen-ljuskälla, en så kallad fri-elektron laser-röntgen (XFEL), är ungefär en miljon gånger starkare än tidigare röntgen-ljuskällor. Eftersom ljusstrålen kommer i korta pulser är det möjligt att göra tidsupplösta experiment ända ner på femtosekund-skala ($10^{-15}$ s). Dock är en bieffekt av den kraftfulla röntgenstrålen vid dessa ljuskällor att proteinkristallen förstörs. Konsekvensen av detta är man behöver tusentals så kallade mikrokristaller för att beräkna proteinets struktur och metoderna för att skapa dessa mikrokristaller är fortfarande relativt outvecklade i jämförelse med normalstora proteinkristaller.

Proteinet som i huvudsak behandlas i den här avhandlingen är ett bakteriellt fotosyntetiskt reaktionscentrum. Detta membranprotein har en central funktion i processen som omvandlar solljus till energi i olika livsformer, till exempel i växter. Proteinet kan absorbera fotoner och startar en elektrontransportkedja inuti membranet vilket leder till produktionen av energirika molekyler som sedan kan användas som bränsle i cellen.

Den första delen av arbetet handlar om att utveckla nya metoder för att kristallisera membranproteiner i mikrokristall-form. Kristalliseringen har utvecklats både för kristallisering i vattenlösningar och för så kallat "lipidisk kubisk fas"; ett slags artificiellt membran bestående av en blandning av fett och vatten med en konsistens liknande vaselin. För att få jämnstora kristaller har proteinet dopats med mikroskopiska korn av redan färdiga kristaller. Dessa korn kan då utgöra en byggsten för tillväxten av nya kristaller och är en bidragande orsak till att många små kristaller bildas istället för några få stora.

Mikrokristallerna har därefter använts för att utföra ett tidsupplöst experiment som gick ut på att ta reda på vad som händer när det fotosyntetiska reaktionscentrumet absorberar ljus. Kristaller i vattenlösning injecerades in i en XFEL-röntgenstråle. Strax innan kristallerna korsade röntgenstrålen besköts de med en laser av samma våglängd där proteinet kan absorbera fotoner. Detta gjorde det möjligt att få strukturell data vid de tidpunkter där elektrontransporten har börjat inne i proteinet och vi kan visa hur atomerna har börjat att röra på sig.

# Chapter 10

# Acknowledgements

**Richard**, thank you for taking me in as a student and believing in me even though I didn't say much. (Unfortunately, I know next to nothing about cricket so I couldn't really fall back on that one as others have done in the past...) I will ruin the fun for you now and say this: The best part of my PhD was seeing diffraction for my LCP crystals (see figure 6.1. ;) ).

**Martin**, thank you for being my examiner and sitting through those boring ISP meetings. Good thing there are more professors now so you don't have to be examiner for everyone.

**Gisela**, thank you being co-supervisor and "adopting" us leftovers into your group meetings. Your advice has been invaluable, if you only knew how many crazy screening projects you've stopped me from doing.

**Rob** thank you being my brother-in-arms on the RC project! Going on all these beamtimes together has been a lot of fun; whether it is drinking sake in tiny local bars in Japan or hunting down lost diabetes equipment in the restaurants of Palo Alto it's always been an adventure. Your enthusiasm and love for Margaritas well make up for the havoc you wreak in the lab!

**Rebecka**, my sister-in-arms since day one! That first summer when we were cloning aquaporins trying to navigate the social circles in the lab as the newbies was one of the best! You taught me that the simple things in life are worth cherishing (the tomato plant is still alive). I will always remember your first week of parental leave when the lunch table was quiet while we all tried to learn how to have normal conversations again.

My office mate and SACLA and Japan travelling partner **Cecilia S**! I thank my lucky star I ended up with you and not anyone else next to me. Hope there's still time for us to have another beamtime trip together, if not we can go somewhere else when it's all over!

**Majolito**, it's as you said, even though we have worked on different things we have shared this time together and I'm really happy we did! I think you are one of the most knowledgeable and kindest persons in the lab, conquering the Swedish

roads will be a walk in the park for you. It's also good to have people you can count on for dancing during the parties!

**Elin D**, I feel I only got to know you in the past year even though we go way back, but now we've gone to Japan and back twice and munched through the entire Lyktan menu together. I love your competitive spirit, your Fia med knuff skills are something special!

**Cecilia W**, it's been great having you as partner for defending! I'm glad your work on the channelrhodopsins paid off now in the end as well, I know how much you've fought for it over the years. Looking forward to some board games later as well as meeting the new addition to the family! (And sorry for always invading your lab bench when you've been stuck with computer work.)

**Elin C**, never stop asking questions! I don't understand half of the things you talk about these days, that's how far you've come! **Léo**, the stylish genius! I wish I had half of your quirkiness, at least I can match your love of cheese..

**Jennie** you taught me EVERYTHING during my first years in the lab. I'm lucky to have had one of the best teachers in the lab, good luck with the new addition to the family! **Kristina** thank you for all of the advice while I was working on the aquaporin project. I think you're one of few people in the lab who have really managed to balance work and family life, hope people can take some inspiration from that! **Florian**, I'm happy you're not all bitterness after passing half-time. All the time that went into knitting the Leia-hat was so. worth. it. **Jessica**, good luck picking up the torch on the fluorescence project. After a half-marathon it should be a piece of cake!

**Ida**, thank you for dragging me along to your choir! I had a lot of fun with you, the journey to Tällberg island will always have a special place in my memories. You also taught me to not take crap from other people and that whisky can be tasty if it's a good one. I hope you and Federico will enjoy baby life together! **Mike**, I don't think I met anyone who loves science and semlas as much as you do, hope you continue enjoying life down under.

**Emil**, **Petra**, **Oskar**, **David**, **Linda**. The real beerclub gang! People don't understand how you can have as many points as you do but that's because of course it's not the same anymore. Never stop with the passive aggressive embroideries, do stop with the stealing of bikes...

**Rhawnie**, thank you for your support, your advice to "just write!!" seemed crazy at the time but it really helped me! (Then I forgot about the book you sent me until everything was done hehe.)

The group: **Rajiv**, **Greger**, **Rob B**, **Daniel**, **Giorgia**, **Per**, **Swagatha**. It's been great working together with you and going on beamtimes together (as well as kidnapping some of you for my experiments when more people were needed). **Owens**, **Jonatan**, **Doris**. Good luck with continuing the oxidase stuff, I can tell you already have a lot of fun together!

The Astra crowd **Andreas** and **Jenny**. I may be leaving soon but the X-ravens live on!

**Gergely**, thank you for helping with processing stuff and with the random Linux troubles when Bruno hasn't been around. **Viktor**, you are also part of the ever-growing RC-blob now, enjoy your parental leave! **Maja**, it's great to have another voice of reason in the lab and a personal source of joy when you are mad at something.

**Tinna**, **Bruno**, **Valida**, **Ingrid** and **Lars**. You guys make this place function. It's a small miracle people can work at all during summer vacations.

The extended Westenhoffs: **Sebastian**, **Weixiao**, **Linnéa**, **Mattÿs**, **Claire**, **Joachim**, **Amke**, **Ann**, **Michal**, **Andrea**, **Leticia**, **Lauras**. It's been great working working with you, joining you for some of your beamtimes and listening to in-depth analysis of snacks.

The basement crowd: **Johanna**, **Björn**, **Emelie**, **Davide**, **Darius**, **Laura**, **Dimitra**, **Ivana**, **Lisa**, **Josh**, **Yilber**, **Damasus**, **Jake**. It's a shame we can't fit on one floor but it's always nice when you join for coffee or beer!

Our collaborators at SACLA and PSI who have always been super-friendly and made us feel like part of their group when we go on beamtimes. Especially **Antonia** who always has time for a coffee and **Thomas** who always has time for a beer.

All the people that have been through the lab in the past: **Ash**, **Stephan**, **Stefan**, **Mikael**, **Alex J**, **Alex B** and last but not least my old office mate **Annette**. It's great to see you from time to time and hope that you are doing well!

With all the people passing through over the years I know that there will be people I remember after this goes to print. For you I can only give my thanks and this classic Swedish line: Ingen nämnd, ingen glömd. Sorry.

Sist men inte minst vill jag tacka min underbara familj. Trots tappra försök att förstå vad det är jag faktiskt har sysslat med genom åren så har ni alltid stöttat mig när jag misslyckats med att förklara. Snart är det slut med runtflängandet!

# Bibliography


[1] J. P. Overington, B. Al-Lazikani, and A. L. Hopkins, "How many drug targets are there?" *Nature Reviews Drug Discovery*, vol. 5, no. 12, pp. 993–996, 2006.

[2] M. A. Yildirim, K. I. Goh, M. E. Cusick, A. L. Barabasi, and M. Vidal, "Drug-target network," *Nature Biotechnology*, vol. 25, no. 10, pp. 1119–1126, 2007.

[3] M. Rask-Andersen, M. S. Almen, and H. B. Schioth, "Trends in the exploitation of novel drug targets," *Nature Reviews Drug Discovery*, vol. 10, no. 8, pp. 579–590, 2011.

[4] D. Voet and J. G. Voet, *Biochemistry*, 4th ed. Hoboken, NJ: John Wiley Sons, 2011.

[5] S. Eberhard, G. Finazzi, and F. A. Wollman, "The dynamics of photosynthesis," *Annual Review of Genetics*, vol. 42, pp. 463–515, 2008.

[6] J. F. Imhoff, *The phototrophic alpha-proteobacteria*. New York, NY: Springer New York, 2006, pp. 41–64.

[7] S. Scheuring, J. Seguin, S. Marco, D. Lévy, B. Robert, and J. L. Rigaud, "Nanodissection and high-resolution imaging of the *Rhodopseudomonas viridis* photosynthetic core complex in native membranes by AFM," *Proceedings of the National Academy of Sciences of the United States of America*, vol. 100, no. 4, pp. 1690–1693, 2003.

[8] P. Qian, C. A. Siebert, P. Wang, D. P. Canniffe, and C. N. Hunter, "Cryo-EM structure of the *Blastochloris viridis* LH1-RC complex at 2.9 Å," *Nature*, vol. 556, no. 7700, pp. 203–208, 2018.

[9] A. G. McEwan, "Photosynthetic electron transport and anaerobic metabolism in purple non-sulfur phototrophic bacteria," *Antonie Van Leeuwenhoek*, vol. 66, no. 1-3, pp. 151–164, 1994.

[10] R. E. Blankenship, *Molecular mechanisms of photosynthesis*, 2nd ed. Chichester, West Sussex: Wiley/Blackwell, 2014.

[11] J. Deisenhofer, O. Epp, K. Miki, R. Huber, and H. Michel, "X-ray structure analysis of a membrane protein complex: Electron density map at 3 Å resolution and a model of the chromophores of the photosynthetic reaction center from *Rhodopseudomonas viridis*," *Journal of Molecular Biology*, vol. 180, no. 2, pp. 385–398, 1984.

[12] ——, "Structure of the protein subunits in the photosynthetic reaction centre of *Rhodopseudomonas viridis* at 3Å resolution," *Nature*, vol. 318, no. 6047, pp. 618–624, 1985.

[13] C. H. Chang, D. Tiede, J. Tang, U. Smith, J. Norris, and M. Schiffer, "Structure of *Rhodopseudomonas sphaeroides* R-26 reaction center," *FEBS Letters*, vol. 205, no. 2, pp. 82–86, 1986.

[14] J. P. Allen, G. Feher, T. O. Yeates, H. Komiya, and D. C. Rees, "Structure of the reaction center from *Rhodobacter sphaeroides* R-26: The cofactors," *Proceedings of the National Academy of Sciences of the United States of America*, vol. 84, no. 16, pp. 5730–5734, 1987.

[15] R. J. Shopes and C. A. Wraight, "Charge recombination from the $P^+Q_A^-$ state in reaction centers from *Rhodopseudomonas viridis*," *Biochimica et Biophysica Acta*, vol. 893, no. 3, pp. 409–425, 1987.

[16] J. M. Ortega and P. Mathis, "Effect of temperature on the kinetics of electron transfer from the tetraheme cytochrome to the primary donor in *Rhodopseudomonas viridis*," *FEBS Letters*, vol. 301, no. 1, pp. 45–48, 1992.

[17] Y. Y. Sham, I. Muegge, and A. Warshel, "Simulating proton translocations in proteins: Probing proton transfer pathways in the *Rhodobacter sphaeroides* reaction center," *Proteins: Structure, Function and Bioinformatics*, vol. 36, no. 4, pp. 484–500, 1999.

[18] M. Y. Okamura, M. L. Paddock, M. S. Graige, and G. Feher, "Proton and electron transfer in bacterial reaction centers," *Biochimica et Biophysica Acta - Bioenergetics*, vol. 1458, no. 1, pp. 148–163, 2000.

[19] G. Feher, J. P. Allen, M. Y. Okamura, and D. C. Rees, "Structure and function of bacterial photosynthetic reaction centers," *Nature*, vol. 339, no. 6220, pp. 111–116, 1989.

[20] A. W. Rutherford and P. Faller, "Photosystem II: evolutionary perspectives," *Philosophical Transactions of the Royal Society B: Biological Sciences*, vol. 358, no. 1429, pp. 245–253, 2003.

[21] T. Cardona, A. Sedoud, N. Cox, and A. W. Rutherford, "Charge separation in photosystem II: A comparative and evolutionary overview," *Biochimica et Biophysica Acta*, vol. 1817, no. 1, pp. 26–43, 2012.

[22] B. Svensson, C. Etchebest, P. Tuffery, P. van Kan, J. Smith, and S. Styring, "A model for the photosystem II reaction center core including the structure of the primary donor $P_{680}$," *Biochemistry*, vol. 35, no. 46, pp. 14 486–14 502, 1996.

[23] J. Xiong, W. M. Fischer, K. Inoue, M. Nakahara, and C. E. Bauer, "Molecular evidence for the early evolution of photosynthesis," *Science*, vol. 289, no. 5485, pp. 1724–1730, 2000.

[24] J. Xiong and C. E. Bauer, "A cytochrome *b* origin of photosynthetic reaction centers: an evolutionary link between respiration and photosynthesis," *Journal of Molecular Biology*, vol. 322, no. 5, pp. 1025–1037, 2002.

[25] J. Breton, J. L. Martin, A. Migus, A. Antonetti, and A. Orszag, "Femtosecond spectroscopy of excitation energy transfer and initial charge separation in the reaction center of the photosynthetic bacterium *Rhodopseudomonas viridis*," *Proceedings of the National Academy of Sciences of the United States of America*, vol. 83, no. 14, pp. 5121–5125, 1986.

[26] J. L. Martin, J. Breton, A. J. Hoff, A. Migus, and A. Antonetti, "Femtosecond spectroscopy of electron-transfer in the reaction center of the photosynthetic bacterium *Rhodopseudomonas sphaeroides* R-26: Direct electron transfer from the dimeric bacteriochlorophyll primary donor to the bacteriopheophytin acceptor with a time constant 2.8 ± 0.2 psec," *Proceedings of the National Academy of Sciences of the United States of America*, vol. 83, no. 4, pp. 957–961, 1986.

[27] M. R. Wasielewski and D. M. Tiede, "Sub-picosecond measurements of primary electron transfer in *Rhodopseudomonas viridis* reaction centers using near-infrared excitation," *FEBS Letters*, vol. 204, no. 2, pp. 368–372, 1986.

[28] W. Zinth, M. C. Nuss, M. A. Franz, W. Kaiser, and H. Michel, *Femtosecond Studies of the Reaction Center of Rhodopsomonas viridis: The Very First Dynamics of the Electron-Transfer Process, Antennas and Reaction Centers of Photosynthetic Bacteria*. Berlin, Heidelberg: Springer, 1985.

[29] W. Holzapfel, U. Finkele, W. Kaiser, D. Oesterhelt, H. Scheer, H. U. Stilz, and W. Zinth, "Observation of a bacteriochlorophyll anion radical during the primary charge separation in a reaction center," *Chemical Physics Letters*, vol. 160, no. 1, pp. 1–7, 1989.

[30] T. Arlt, S. Schmidt, W. Kaiser, C. Lauterwasser, M. Meyer, H. Scheer, and W. Zinth, "The accessory bacteriochlorophyll: A real electron carrier in primary photosynthesis," *Proceedings of the National Academy of Sciences of the United States of America*, vol. 90, no. 24, pp. 11 757–11 761, 1993.

[31] M. M. Leonova, T. Y. Fufina, L. G. Vasilieva, and V. A. Shuvalov, "Structure-function investigations of bacterial photosynthetic reaction centers," *Biochemistry (Moscow)*, vol. 76, no. 13, pp. 1465–1483, 2011.

[32] M. H. Stowell, T. M. McPhillips, D. C. Rees, S. M. Soltis, E. Abresch, and G. Feher, "Light-induced structural changes in photosynthetic reaction center: Implications for mechanism of electron-proton transfer," *Science*, vol. 276, no. 5313, pp. 812–816, 1997.

[33] J. Breton, "Absence of large-scale displacement of quinone $Q_B$ in bacterial photosynthetic reaction centers," *Biochemistry*, vol. 43, no. 12, pp. 3318–3326, 2004.

[34] R. H. G. Baxter, B. L. Seagle, N. Ponomarenko, and J. R. Norris, "Cryogenic structure of the photosynthetic reaction center of *Blastochloris viridis* in the light and dark," *Acta Crystallographica Section D: Structural Biology*, vol. 61, pp. 605–612, 2005.

[35] C. R. D. Lancaster and H. Michel, "The coupling of light-induced electron transfer and proton uptake as derived from crystal structures of reaction centres from *Rhodopseudomonas viridis* modified at the binding site of the secondary quinone, $Q_B$," *Structure*, vol. 5, no. 10, pp. 1339–1359, 1997.

[36] R. A. Marcus, "On the theory of oxidation-reduction reactions involving electron transfer I," *The Journal of Chemical Physics*, vol. 24, no. 5, pp. 966–978, 1956.

[37] R. A. Marcus and N. Sutin, "Electron transfers in chemistry and biology," *Biochimica et Biophysica Acta*, vol. 811, no. 3, pp. 265–322, 1985.

[38] C. A. Wraight and R. K. Clayton, "The absolute quantum efficiency of bacteriochlorophyll photooxidation in reaction centers of *Rhodopseudomonas spheroides*," *Biochimica et Biophysica Acta*, vol. 333, no. 2, pp. 246–260, 1974.

[39] G. R. Fleming, J. L. Martin, and J. Breton, "Rates of primary electron transfer in photosynthetic reaction centers and their mechanistic implications," *Nature*, vol. 333, no. 6169, pp. 190–192, 1988.

[40] H. Y. Wang, S. Lin, J. P. Allen, J. C. Williams, S. Blankert, C. Laser, and N. W. Woodbury, "Protein dynamics control the kinetics of initial electron transfer in photosynthesis," *Science*, vol. 316, no. 5825, pp. 747–750, 2007.

[41] V. Vagenende, M. G. S. Yap, and B. L. Trout, "Mechanisms of protein stabilization and prevention of protein aggregation by glycerol," *Biochemistry*, vol. 48, no. 46, pp. 11 084–11 096, 2009.

[42] F. Mancia and J. Love, "High-throughput expression and purification of membrane proteins," *Journal of Structural Biology*, vol. 172, no. 1, pp. 85–93, 2010.

[43] G. G. Privé, "Detergents for the stabilization and crystallization of membrane proteins," *Methods*, vol. 41, no. 4, pp. 388–397, 2007.

[44] C. L. Young, Z. T. Britton, and A. S. Robinson, "Recombinant protein expression and purification: A comprehensive review of affinity tags and microbial applications," *Biotechnology Journal*, vol. 7, no. 5, pp. 620–634, 2012.

[45] M. Konorty, V. Brumfeld, A. Vermeglio, N. Kahana, O. Medalia, and A. Minsky, "Photosynthetic system in *Blastochloris viridis* revisited," *Biochemistry*, vol. 48, no. 22, pp. 4753–4761, 2009.

[46] J. Eccles, B. Honig, and K. Schulten, "Spectroscopic determinants in the reaction center of *Rhodopseudomonas viridis*," *Biophysical Journal*, vol. 53, no. 2, pp. 137–144, 1988.

[47] N. E. Chayen, "Recent advances in methodology for the crystallization of biological macromolecules," *Journal of Crystal Growth*, vol. 198, pp. 649–655, 1999.

[48] J. A. Gavira, "Current trends in protein crystallization," *Archives of Biochemistry and Biophysics*, vol. 602, pp. 3–11, 2016.

[49] N. Asherie, "Protein crystallization and phase diagrams," *Methods*, vol. 34, no. 3, pp. 266–272, 2004.

[50] L. Griffin and A. Lawson, "Antibody fragments as tools in crystallography," *Clinical and Experimental Immunology*, vol. 165, no. 3, pp. 285–291, 2011.

[51] C. Hunte and H. Michel, "Crystallisation of membrane proteins mediated by antibody fragments," *Current Opinion in Structural Biology*, vol. 12, no. 4, pp. 503–508, 2002.

[52] P. Gast, P. Hemelrijk, and A. J. Hoff, "Determination of the number of detergent molecules associated with the reaction center protein isolated from the photosynthetic bacterium *Rhodopseudomonas viridis*: Effects of the amphiphilic molecule 1,2,3-heptanetriol," *FEBS Letters*, vol. 337, no. 1, pp. 39–42, 1994.

[53] E. M. Landau and J. P. Rosenbusch, "Lipidic cubic phases: A novel concept for the crystallization of membrane proteins," *Proceedings of the National Academy of Sciences of the United States of America*, vol. 93, no. 25, pp. 14 532–14 535, 1996.

[54] D. Li, J. Lee, and M. Caffrey, "Crystallizing membrane proteins in lipidic mesophases. A host lipid screen," *Crystal Growth Design*, vol. 11, no. 2, pp. 530–537, 2011.

[55] V. Cherezov, J. Clogston, Y. Misquitta, W. Abdel-Gawad, and M. Caffrey, "Membrane protein crystallization in meso: Lipid type-tailoring of the cubic phase," *Biophysical Journal*, vol. 83, no. 6, pp. 3393–3407, 2002.

[56] Y. Misquitta and M. Caffrey, "Detergents destabilize the cubic phase of monoolein: Implications for membrane protein crystallization," *Biophysical Journal*, vol. 85, no. 5, pp. 3084–3096, 2003.

[57] P. Wadsten, A. B. Wöhri, A. Snijder, G. Katona, A. T. Gardiner, R. J. Cogdell, R. Neutze, and S. Engström, "Lipidic sponge phase crystallization of membrane proteins," *Journal of Molecular Biology*, vol. 364, no. 1, pp. 44–53, 2006.

[58] V. Cherezov, J. Clogston, M. Z. Papiz, and M. Caffrey, "Room to move: Crystallizing membrane proteins in swollen lipidic mesophases," *Journal of Molecular Biology*, vol. 357, no. 5, pp. 1605–1618, 2006.

[59] P. Nollert and E. M. Landau, "Enzymic release of crystals from lipidic cubic phases," *Biochemical Society Transactions*, vol. 26, no. 4, pp. 709–713, 1998.

[60] W. H. Bragg and W. L. Bragg, "The reflection of X-rays by crystals." *Proceedings of the Royal Society A: Mathematical, Physical and Engineering Sciences*, vol. 88, no. 605, pp. 428–438, 1913.

[61] P. P. Ewald, "Introduction to dynamical theory of X-ray diffraction," *Acta Crystallographica Section A: Foundations and Advances*, vol. 25, pp. 103–109, 1969.

[62] A. G. W. Leslie, "The integration of macromolecular diffraction data," *Acta Crystallographica Section D: Structural Biology*, vol. 62, pp. 48–57, 2006.

[63] T. G. G. Battye, L. Kontogiannis, O. Johnson, H. R. Powell, and A. G. W. Leslie, "iMOSFLM: a new graphical interface for diffraction-image processing with MOSFLM," *Acta Crystallographica Section D: Structural Biology*, vol. 67, pp. 271–281, 2011.

[64] W. Kabsch, "XDS," *Acta Crystallographica Section D: Structural Biology*, vol. 66, pp. 125–132, 2010.

[65] A. Patterson, "A direct method for the determination of the components of interatomic distances in crystals," *Zeitschrift für Kristallographie - Crystalline Materials*, vol. 90, no. 1-6, pp. 517–542, 1935.

[66] G. J. Kleywegt, "Validation of protein crystal structures," *Acta Crystallographica Section D: Structural Biology*, vol. 56, pp. 249–265, 2000.

[67] A. L. Lamb, T. J. Kappock, and N. R. Silvaggi, "You are lost without a map: Navigating the sea of protein structures," *Biochimica et Biophysica Acta - Proteins and Proteomics*, vol. 1854, no. 4, pp. 258–268, 2015.

[68] G. N. Ramachandran, C. Ramakrishnan, and V. Sasisekharan, "Stereochemistry of polypeptide chain configurations," *Journal of Molecular Biology*, vol. 7, no. 1, pp. 95–99, 1963.

[69] R. Henderson, "Cryo-protection of protein crystals against radiation damage in electron and X-ray-diffraction," *Proceedings of the Royal Society B: Biological Sciences*, vol. 241, no. 1300, pp. 6–8, 1990.

[70] B. Heras and J. L. Martin, "Post-crystallization treatments for improving diffraction quality of protein crystals," *Acta Crystallographica Section D: Structural Biology*, vol. 61, pp. 1173–1180, 2005.

[71] H. Ihee, M. Wulff, J. Kim, and S. Adachi, "Ultrafast X-ray scattering: Structural dynamics from diatomic to protein molecules," *International Reviews in Physical Chemistry*, vol. 29, no. 3, pp. 453–520, 2010.

[72] M. Levantino, B. A. Yorke, D. C. F. Monteiro, M. Cammarata, and A. R. Pearson, "Using synchrotrons and XFELs for time-resolved X-ray crystallography and solution scattering experiments on biomolecules," *Current Opinion in Structural Biology*, vol. 35, pp. 41–48, 2015.

[73] R. Neutze, R. Wouts, D. van der Spoel, E. Weckert, and J. Hajdu, "Potential for biomolecular imaging with femtosecond X-ray pulses," *Nature*, vol. 406, no. 6797, pp. 752–757, 2000.

[74] H. N. Chapman, P. Fromme, A. Barty, T. A. White, R. A. Kirian, A. Aquila, M. S. Hunter, J. Schulz, D. P. DePonte, U. Weierstall, R. B. Doak, F. R. N. C. Maia, A. V. Martin, I. Schlichting, L. Lomb, N. Coppola, R. L. Shoeman, S. W. Epp, R. Hartmann, D. Rolles, A. Rudenko, L. Foucar, N. Kimmel, G. Weidenspointner, P. Holl, M. N. Liang, M. Barthelmess, C. Caleman, S. Boutet, M. J. Bogan, J. Krzywinski, C. Bostedt, S. Bajt, L. Gumprecht, B. Rudek, B. Erk, C. Schmidt, A. Hömke, C. Reich, D. Pietschner, L. Strüder, G. Hauser, H. Gorke, J. Ullrich, S. Herrmann, G. Schaller, F. Schopper, H. Soltau, K. U. Kühnel, M. Messerschmidt, J. D. Bozek, S. P. Hau-Riege, M. Frank, C. Y. Hampton, R. G. Sierra, D. Starodub, G. J. Williams, J. Hajdu, N. Timneanu, M. M. Seibert, J. Andreasson, A. Rocker, O. Jönsson, M. Svenda, S. Stern, K. Nass, R. Andritschke, C. D. Schröter, F. Krasniqi, M. Bott, K. E. Schmidt, X. Y. Wang, I. Grotjohann, J. M. Holton, T. R. M. Barends, R. Neutze, S. Marchesini, R. Fromme, S. Schorb, D. Rupp, M. Adolph, T. Gorkhover, I. Andersson, H. Hirsemann, G. Potdevin, H. Graafsma, B. Nilsson, and J. C. H. Spence, "Femtosecond X-ray protein nanocrystallography," *Nature*, vol. 470, no. 7332, pp. 73–78, 2011.

[75] D. P. DePonte, U. Weierstall, K. Schmidt, J. Warner, D. Starodub, J. C. H. Spence, and R. B. Doak, "Gas dynamic virtual nozzle for generation of microscopic droplet streams," *Journal of Physics D: Applied Physics*, vol. 41, no. 19, 2008.

[76] R. G. Sierra, H. Laksmono, J. Kern, R. Tran, J. Hattne, R. Alonso-Mori, B. Lassalle-Kaiser, C. Glöckner, J. Hellmich, D. W. Schafer, N. Echols, R. J. Gildea, R. W. Grosse-Kunstleve, J. Sellberg, T. A. McQueen, A. R. Fry, M. M. Messerschmidt, A. Miahnahri, M. M. Seibert, C. Y. Hampton, D. Starodub, N. D. Loh, D. Sokaras, T. C. Weng, P. H. Zwart, P. Glatzel, D. Milathianaki, W. E. White, P. D. Adams, G. J. Williams, S. Boutet, A. Zouni, J. Messinger, N. K. Sauter, U. Bergmann, J. Yano, V. K. Yachandra, and M. J. Bogan, "Nanoflow electrospinning serial femtosecond crystallography," *Acta Crystallographica Section D: Structural Biology*, vol. 68, pp. 1584–1587, 2012.

[77] C. G. Roessler, R. Agarwal, M. Allaire, R. Alonso-Mori, B. Andi, J. F. R. Bachega, M. Bommer, A. S. Brewster, M. C. Browne, R. Chatterjee, E. Cho, A. E. Cohen, M. Cowan, S. Datwani, V. L. Davidson, J. Defever, B. Eaton, R. Ellson, Y. P. Feng, L. P. Ghislain, J. M. Glownia, G. Y. Han, J. Hattne, J. Hellmich, A. Héroux, M. Ibrahim, J. Kern, A. Kuczewski, H. T. Lemke, P. H. Liu, L. Majlof, W. M. McClintock, S. Myers, S. Nelsen, J. Olechno, A. M. Orville, N. K. Sauter, A. S. Soares, S. M. Soltis, H. Song, R. G. Stearns, R. Tran, Y. Tsai, M. Uervirojnangkoorn, C. M. Wilmot, V. Yachandra, J. Yano, E. T. Yukl, D. L. Zhu, and A. Zouni, "Acoustic injectors for drop-on-demand serial femtosecond crystallography," *Structure*, vol. 24, no. 4, pp. 631–640, 2016.

[78] U. Weierstall, D. James, C. Wang, T. A. White, D. J. Wang, W. Liu, J. C. H. Spence, R. B. Doak, G. Nelson, P. Fromme, R. Fromme, I. Grotjohann, C. Kupitz, N. A. Zatsepin, H. G. Liu, S. Basu, D. Wacker, G. W. Han, V. Katritch, S. Boutet, M. Messerschmidt, G. J. Williams, J. E. Koglin, M. M. Seibert, M. Klinker, C. Gati, R. L. Shoeman, A. Barty, H. N. Chapman, R. A. Kirian, K. R. Beyerlein, R. C. Stevens, D. F. Li, S. T. A. Shah, N. Howe, M. Caffrey, and V. Cherezov, "Lipidic cubic phase injector facilitates membrane protein serial femtosecond crystallography," *Nature Communications*, vol. 5, 2014.

[79] S. Botha, K. Nass, T. R. M. Barends, W. Kabsch, B. Latz, F. Dworkowski, L. Foucar, E. Panepucci, M. T. Wang, R. L. Shoeman, I. Schlichting, and R. B. Doak, "Room-temperature serial crystallography at synchrotron X-ray sources using slowly flowing free-standing high-viscosity microstreams," *Acta Crystallographica Section D: Structural Biology*, vol. 71, pp. 387–397, 2015.

[80] W. Liu, A. Ishchenko, and V. Cherezov, "Preparation of microcrystals in lipidic cubic phase for serial femtosecond crystallography," *Nature Protocols*, vol. 9, no. 9, pp. 2123–2134, 2014.

[81] M. Sugahara, E. Mizohata, E. Nango, M. Suzuki, T. Tanaka, T. Masuda, R. Tanaka, T. Shimamura, Y. Tanaka, C. Suno, K. Ihara, D. Pan, K. Kakinouchi, S. Sugiyama, M. Murata, T. Inoue, K. Tono, C. Song, J. Park, T. Kameshima, T. Hatsui, Y. Joti, M. Yabashi, and S. Iwata, "Grease matrix as a versatile carrier of proteins for serial crystallography," *Nature Methods*, vol. 12, no. 1, pp. 61–63, 2015.

[82] C. E. Conrad, S. Basu, D. James, D. Wang, A. Schaffer, S. Roy-Chowdhury, N. A. Zatsepin, A. Aquila, J. Coe, C. Gati, M. S. Hunter, J. E. Koglin, C. Kupitz, G. Nelson, G. Subramanian, T. A. White, Y. Zhao, J. Zook, S. Boutet, V. Cherezov, J. C. Spence, R. Fromme, U. Weierstall, and P. Fromme, "A novel inert crystal delivery medium for serial femtosecond crystallography," *IUCrJ*, vol. 2, no. Pt 4, pp. 421–430, 2015.

[83] M. Sugahara, C. Song, M. Suzuki, T. Masuda, S. Inoue, T. Nakane, F. Yumoto, E. Nango, R. Tanaka, K. Tono, Y. Joti, T. Kameshima, T. Hatsui, M. Yabashi, O. Nureki, K. Numata, and S. Iwata, "Oil-free hyaluronic acid matrix for serial femtosecond crystallography," *Scientific Reports*, vol. 6, 2016.

[84] M. Sugahara, T. Nakane, T. Masuda, M. Suzuki, S. Inoue, C. Song, R. Tanaka, T. Nakatsu, E. Mizohata, F. Yumoto, K. Tono, Y. Joti, T. Kameshima, T. Hatsui, M. Yabashi, O. Nureki, K. Numata, E. Nango, and S. Iwata, "Hydroxyethyl cellulose matrix applied to serial crystallography," *Scientific Reports*, vol. 7, 2017.

[85] J. Park, S. Park, J. Kim, G. Park, Y. Cho, and K. H. Nam, "Polyacrylamide injection matrix for serial femtosecond crystallography," *Scientific Reports*, vol. 9, 2019.

[86] D. James, "Injection methods and instrumentation for serial X-ray free electron laser experiments," Doctoral thesis, Arizona State University, 2015.

[87] D. J. Wang, U. Weierstall, L. Pollack, and J. Spence, "Double-focusing mixing jet for XFEL study of chemical kinetics," *Journal of Synchrotron Radiation*, vol. 21, pp. 1364–1366, 2014.

[88] D. Oberthuer, J. Knoška, M. O. Wiedorn, K. R. Beyerlein, D. A. Bushnell, E. G. Kovaleva, M. Heymann, L. Gumprecht, R. A. Kirian, A. Barty, V. Mariani, A. Tolstikova, L. Adriano, S. Awel, M. Barthelmess, K. Dörner, P. L. Xavier, O. Yefanov, D. R. James, G. Nelson, D. J. Wang, G. Calvey, Y. J. Chen, A. Schmidt, M. Szczepek, S. Frielingsdorf, O. Lenz, E. Snell, P. J. Robinson, B. Šarler, G. Belšak, M. Maček, F. Wilde, A. Aquila, S. Boutet, M. N. Liang, M. S. Hunter, P. Scheerer, J. D. Lipscomb, U. Weierstall, R. D. Kornberg, J. C. H. Spence, L. Pollack, H. N. Chapman, and S. Bajt, "Double-flow focused liquid injector for efficient serial femtosecond crystallography," *Scientific Reports*, vol. 7, 2017.

[89] C. H. Yoon and T. A. White, *Climbing the Data Mountain: Processing of SFX Data*. Cham: Springer International Publishing, 2018, pp. 209–233.

[90] T. A. White, "Post-refinement method for snapshot serial crystallography," *Philosophical Transactions of the Royal Society B: Biological Sciences*, vol. 369, 2014.

[91] M. Uervirojnangkoorn, O. B. Zeldin, A. Y. Lyubimov, J. Hattne, A. S. Brewster, N. K. Sauter, A. T. Brunger, and W. I. Weis, "Enabling X-ray free electron laser crystallography for challenging biological systems from a limited number of crystals," *eLife*, vol. 4, 2015.

[92] P. A. Karplus and K. Diederichs, "Linking crystallographic model and data quality," *Science*, vol. 336, no. 6084, pp. 1030–1033, 2012.

[93] A. J. McCoy, R. W. Grosse-Kunstleve, P. D. Adams, M. D. Winn, L. C. Storoni, and R. J. Read, "Phaser crystallographic software," *Journal of Applied Crystallography*, vol. 40, pp. 658–674, 2007.

[94] M. D. Winn, C. C. Ballard, K. D. Cowtan, E. J. Dodson, P. Emsley, P. R. Evans, R. M. Keegan, E. B. Krissinel, A. G. W. Leslie, A. McCoy, S. J. McNicholas, G. N. Murshudov, N. S. Pannu, E. A. Potterton, H. R. Powell, R. J. Read, A. Vagin, and K. S. Wilson, "Overview of the *CCP*4 suite and current developments," *Acta Crystallographica Section D: Structural Biology*, vol. 67, pp. 235–242, 2011.

[95] P. V. Afonine, R. W. Grosse-Kunstleve, N. Echols, J. J. Headd, N. W. Moriarty, M. Mustyakimov, T. C. Terwilliger, A. Urzhumtsev, P. H. Zwart, and P. D. Adams, "Towards automated crystallographic structure refinement with *phenix.refine*," *Acta Crystallographica Section D: Structural Biology*, vol. 68, pp. 352–367, 2012.

[96] M. S. Hunter, C. H. Yoon, H. DeMirci, R. G. Sierra, E. H. Dao, R. Ahmadi, F. Aksit, A. L. Aquila, H. Ciftci, S. Guillet, M. J. Hayes, T. J. Lane, M. Liang, U. Lundstrom, J. E. Koglin, P. Mgbam, Y. Rao, L. Zhang, S. Wakatsuki, J. M. Holton, and S. Boutet, "Selenium single-wavelength anomalous diffraction *de novo* phasing using an X-ray-free electron laser," *Nature Communications*, vol. 7, 2016.

[97] K. Yamashita, N. Kuwabara, T. Nakane, T. Murai, E. Mizohata, M. Sugahara, D. Q. Pan, T. Masuda, M. Suzuki, T. Sato, A. Kodan, T. Yamaguchi, E. Nango, T. Tanaka, K. Tono, Y. Joti, T. Kameshima, T. Hatsui, M. Yabashi, H. Manya, T. Endo, R. Kato, T. Senda, H. Kato, S. Iwata, H. Ago, M. Yamamoto, F. Yumoto, and T. Nakatsu, "Experimental phase determination with selenomethionine or mercury-derivatization in serial femtosecond crystallography," *IUCrJ*, vol. 4, pp. 639–647, 2017.

[98] P. Hart, S. Boutet, G. Carini, M. Dubrovin, B. Duda, D. Fritz, G. Haller, R. Herbst, S. Herrmann, C. Kenney, N. Kurita, H. Lemke, M. Messerschmidt, M. Nordby, J. Pines, D. Schafer, M. Swift, M. Weaver, G. Williams, D. L. Zhu, N. Van Bakel, and J. Morse, "The CSPAD megapixel x-ray camera at LCLS," *Proceedings of SPIE*, vol. 8504, 2012.

[99] T. Kameshima, S. Ono, T. Kudo, K. Ozaki, Y. Kirihara, K. Kobayashi, Y. Inubushi, M. Yabashi, T. Horigome, A. Holland, K. Holland, D. Burt, H. Murao, and T. Hatsui, "Development of an X-ray pixel detector with multi-port charge-coupled device for X-ray free-electron laser experiments," *Review of Scientific Instruments*, vol. 85, no. 3, 2014.

[100] J. Schwandt, E. Fretwurst, R. Klanner, and J. Zhang, "Design of the AGIPD sensor for the european XFEL," *Journal of Instrumentation*, vol. 8, 2013.

[101] M. Harmand, R. Coffee, M. R. Bionta, M. Chollet, D. French, D. Zhu, D. M. Fritz, H. T. Lemke, N. Medvedev, B. Ziaja, S. Toleikis, and M. Cammarata, "Achieving few-femtosecond time-sorting at hard X-ray free-electron lasers," *Nature Photonics*, vol. 7, no. 3, pp. 215–218, 2013.

[102] K. Nakajima, Y. Joti, T. Katayama, S. Owada, T. Togashi, T. Abe, T. Kameshima, K. Okada, T. Sugimoto, M. Yamaga, T. Hatsui, and M. Yabashi, "Software for the data analysis of the arrival-timing monitor at SACLA," *Journal of Synchrotron Radiation*, vol. 25, pp. 592–603, 2018.

[103] D. Arnlund, "X-ray free-electron laser based methods for structural and ultrafast dynamics studies of a photo-synthetic reaction centre," Doctoral thesis, University of Gothenburg, 2014.

[104] T. Ursby and D. Bourgeois, "Improved estimation of structure-factor difference amplitudes from poorly accurate data," *Acta Crystallographica Section A: Foundations and Advances*, vol. 53, pp. 564–575, 1997.

[105] A. Y. Lyubimov, T. D. Murray, A. Koehl, I. E. Araci, M. Uervirojnangkoorn, O. B. Zeldin, A. E. Cohen, S. M. Soltis, E. L. Baxter, A. S. Brewster, N. K. Sauter, A. T. Brunger, and J. M. Berger, "Capture and X-ray diffraction studies of protein microcrystals in a microfluidic trap array," *Acta Crystallographica Section D: Structural Biology*, vol. 71, pp. 928–940, 2015.

[106] E. L. Baxter, L. Aguila, R. Alonso-Mori, C. O. Barnes, C. A. Bonagura, W. Brehmer, A. T. Brunger, G. Calero, T. T. Caradoc-Davies, R. Chatterjee, W. F. Degrado, J. S. Fraser, M. Ibrahim, J. Kern, B. K. Kobilka, A. C. Kruse, K. M. Larsson, H. T. Lemke, A. Y. Lyubimov, A. Manglik, S. E. McPhillips, E. Norgren, S. S. Pang, S. M. Soltis, J. H. Song, J. Thomaston, Y. Tsai, W. I. Weis, R. A. Woldeyes, V. Yachandra, J. Yano, A. Zouni, and A. E. Cohen, "High-density grids for efficient data collection from multiple crystals," *Acta Crystallographica Section D: Structural Biology*, vol. 72, pp. 2–11, 2016.

[107] R. B. Doak, G. N. Kovacs, A. Gorel, L. Foucar, T. R. M. Barends, M. L. Grünbein, M. Hilpert, M. Kloos, C. M. Roome, R. L. Shoeman, M. Stricker, K. Tono, D. You, K. Ueda, D. A. Sherrell, R. L. Owen, and I. Schlichting, "Crystallography on a chip - without the chip: sheet-on-sheet sandwich," *Acta Crystallographica Section D: Structural Biology*, vol. 74, pp. 1000–1007, 2018.

[108] C. Kupitz, S. Basu, I. Grotjohann, R. Fromme, N. A. Zatsepin, K. N. Rendek, M. S. Hunter, R. L. Shoeman, T. A. White, D. J. Wang, D. James, J. H. Yang, D. E. Cobb, B. Reeder, R. G. Sierra, H. G. Liu, A. Barty, A. L. Aquila, D. Deponte, R. A. Kirian, S. Bari, J. J. Bergkamp, K. R. Beyerlein, M. J. Bogan, C. Caleman, T. C. Chao, C. E. Conrad, K. M. Davis, H. Fleckenstein, L. Galli, S. P. Hau-Riege, S. Kassemeyer, H. Laksmono, M. N. Liang, L. Lomb, S. Marchesini, A. V. Martin, M. Messerschmidt, D. Milathianaki, K. Nass, A. Ros, S. Roy-Chowdhury, K. Schmidt, M. Seibert, J. Steinbrener, F. Stellato, L. F. Yan, C. Yoon, T. A. Moore, A. L. Moore, Y. Pushkar, G. J. Williams, S. Boutet, R. B. Doak, U. Weierstall, M. Frank, H. N. Chapman, J. C. H. Spence, and P. Fromme, "Serial time-resolved crystallography of photosystem II using a femtosecond X-ray laser," *Nature*, vol. 513, no. 7517, pp. 261–265, 2014.

[109] J. Lu, X. J. Wang, and C. B. Ching, "Batch crystallization of soluble proteins: effect of precipitant, temperature and additive," *Progress in Crystal Growth and Characterization of Materials*, vol. 45, no. 3, pp. 201–217, 2002.

[110] D. B. Lee, J. M. Kim, J. H. Seok, J. H. Lee, J. D. Jo, J. Y. Mun, C. Conrad, J. Coe, G. Nelson, B. Hogue, T. A. White, N. Zatsepin, U. Weierstall, A. Barty, H. Chapman, P. Fromme, J. Spence, M. S. Chung, C. H. Oh, and K. H. Kim, "Supersaturation-controlled microcrystallization and visualization analysis for serial femtosecond crystallography," *Scientific Reports*, vol. 8, 2018.

[111] C. Darmanin, J. Strachan, C. G. Adda, T. Ve, B. Kobe, and B. Abbey, "Protein crystal screening and characterization for serial femtosecond nanocrystallography," *Scientific Reports*, vol. 6, 2016.

[112] L. C. Johansson, D. Arnlund, T. A. White, G. Katona, D. P. Deponte, U. Weierstall, R. B. Doak, R. L. Shoeman, L. Lomb, E. Malmerberg, J. Davidsson, K. Nass, M. Liang, J. Andreasson, A. Aquila, S. Bajt, M. Barthelmess, A. Barty, M. J. Bogan, C. Bostedt, J. D. Bozek, C. Caleman, R. Coffee, N. Coppola, T. Ekeberg, S. W. Epp, B. Erk, H. Fleckenstein, L. Foucar, H. Graafsma, L. Gumprecht, J. Hajdu, C. Y. Hampton, R. Hartmann, A. Hartmann, G. Hauser, H. Hirsemann, P. Holl, M. S. Hunter, S. Kassemeyer, N. Kimmel, R. A. Kirian, F. R. Maia, S. Marchesini, A. V. Martin, C. Reich, D. Rolles, B. Rudek, A. Rudenko, I. Schlichting, J. Schulz, M. M. Seibert, R. G. Sierra, H. Soltau, D. Starodub, F. Stellato, S. Stern, L. Strüder, N. Timneanu, J. Ullrich, W. Y. Wahlgren, X. Wang, G. Weidenspointner, C. Wunderer, P. Fromme, H. N. Chapman, J. C. Spence, and R. Neutze, "Lipidic phase membrane protein serial femtosecond crystallography," *Nature Methods*, vol. 9, no. 3, pp. 263–265, 2012.

[113] L. C. Johansson, D. Arnlund, G. Katona, T. A. White, A. Barty, D. P. DePonte, R. L. Shoeman, C. Wickstrand, A. Sharma, G. J. Williams, A. Aquila, M. J. Bogan, C. Caleman, J. Davidsson, R. B. Doak, M. Frank, R. Fromme, L. Galli, I. Grotjohann, M. S. Hunter, S. Kassemeyer, R. A. Kirian, C. Kupitz, M. Liang, L. Lomb, E. Malmerberg, A. V. Martin, M. Messerschmidt, K. Nass, L. Redecke, M. M. Seibert, J. Sjöhamn, J. Steinbrener, F. Stellato, D. Wang, W. Y. Wahlgren, U. Weierstall, S. Westenhoff, N. A. Zatsepin, S. Boutet, J. C. Spence, I. Schlichting, H. N. Chapman, P. Fromme, and R. Neutze, "Structure of a photosynthetic reaction centre determined by serial femtosecond crystallography," *Nature Communications*, vol. 4, 2013.

[114] H. Michel, "Three-dimensional crystals of a membrane protein complex: The photosynthetic reaction centre from *Rhodopseudomonas viridis*," *Journal of Molecular Biology*, vol. 158, no. 3, pp. 567–572, 1982.

[115] T. Bergfors, "Seeds to crystals," *Journal of Structural Biology*, vol. 142, no. 1, pp. 66–76, 2003.

[116] B. L. Nannenga, D. Shi, A. G. W. Leslie, and T. Gonen, "High-resolution structure determination by continuous-rotation data collection in microED," *Nature Methods*, vol. 11, no. 9, pp. 927–930, 2014.

[117] L. Li, D. Mustafi, Q. Fu, V. Tereshko, D. L. L. Chen, J. D. Tice, and R. F. Ismagilov, "Nanoliter microfluidic hybrid method for simultaneous screening and optimization validated with crystallization of membrane proteins," *Proceedings of the National Academy of Sciences of the United States of America*, vol. 103, no. 51, pp. 19 243–19 248, 2006.

[118] A. W. Roszak, V. Moulisová, A. D. P. Reksodipuro, A. T. Gardiner, R. Fujii, H. Hashimoto, N. W. Isaacs, and R. J. Cogdell, "New insights into the structure of the reaction centre from *Blastochloris viridis*: evolution in the laboratory," *Biochemical Journal*, vol. 442, pp. 27–37, 2012.

[119] C. R. D. Lancaster, M. V. Bibikova, P. Sabatino, D. Oesterhelt, and H. Michel, "Structural basis of the drastically increased initial electron transfer rate in the reaction center from a *Rhodopseudomonas viridis* mutant described at 2.00-Å resolution," *Journal of Biological Chemistry*, vol. 275, no. 50, pp. 39 364–39 368, 2000.

[120] M. Ibrahim, R. Chatterjee, J. Hellmich, R. Tran, M. Bommer, V. K. Yachandra, J. Yano, J. Kern, and A. Zouni, "Improvements in serial femtosecond crystallography of photosystem II by optimizing crystal uniformity using microseeding procedures," *Structural Dynamics*, vol. 2, no. 4, 2015.

[121] L. Lomb, J. Steinbrener, S. Bari, D. Beisel, D. Berndt, C. Kieser, M. Lukat, N. Neef, and R. L. Shoeman, "An anti-settling sample delivery instrument for serial femtosecond crystallography," *Journal of Applied Crystallography*, vol. 45, pp. 674–678, 2012.

[122] G. Blaj, P. Caragiulo, G. Carini, S. Carron, A. Dragone, D. Freytag, G. Haller, P. Hart, J. Hasi, R. Herbst, S. Herrmann, C. Kenney, B. Markovic, K. Nishimura, S. Osier, J. Pines, B. Reese, J. Segal, A. Tomada, and M. Weaver, "X-ray detectors at the Linac Coherent Light Source," *Journal of Synchrotron Radiation*, vol. 22, no. 3, pp. 577–583, 2015.

[123] A. Barty, R. A. Kirian, F. R. N. C. Maia, M. Hantke, C. H. Yoon, T. A. White, and H. Chapman, "*Cheetah*: software for high-throughput reduction and analysis of serial femtosecond X-ray diffraction data," *Journal of Applied Crystallography*, vol. 47, pp. 1118–1131, 2014.

[124] O. Yefanov, V. Mariani, C. Gati, T. A. White, H. N. Chapman, and A. Barty, "Accurate determination of segmented X-ray detector geometry," *Optics Express*, vol. 23, no. 22, pp. 28 459–28 470, 2015.

[125] T. A. White, R. A. Kirian, A. V. Martin, A. Aquila, K. Nass, A. Barty, and H. N. Chapman, "*CrystFEL*: a software suite for snapshot serial crystallography," *Journal of Applied Crystallography*, vol. 45, pp. 335–341, 2012.

[126] A. J. M. Duisenberg, "Indexing in single-crystal diffractometry with an obstinate list of reflections," *Journal of Applied Crystallography*, vol. 25, pp. 92–96, 1992.

[127] S. French and K. Wilson, "On the treatment of negative intensity observations," *Acta Crystallographica Section A: Foundations and Advances*, vol. 34, pp. 517–525, 1978.

[128] G. N. Murshudov, A. A. Vagin, and E. J. Dodson, "Refinement of macromolecular structures by the maximum-likelihood method," *Acta Crystallographica Section D: Structural Biology*, vol. 53, pp. 240–255, 1997.

[129] P. Emsley and K. Cowtan, "*Coot*: model-building tools for molecular graphics," *Acta Crystallographica Section D: Structural Biology*, vol. 60, pp. 2126–2132, 2004.

[130] J. M. Schieferstein, A. S. Pawate, M. J. Varel, S. Guha, I. Astrauskaite, R. B. Gennis, and P. J. A. Kenis, "X-ray transparent microfluidic platforms for membrane protein crystallization with microseeds," *Lab on a Chip*, vol. 18, no. 6, pp. 944–954, 2018.

[131] P. Gast, T. J. Michalski, J. E. Hunt, and J. R. Norris, "Determination of the amount and the type of quinones present in single crystals from reaction center protein from the photosynthetic bacterium *Rhodopseudomonas viridis*," *FEBS Letters*, vol. 179, no. 2, pp. 325–328, 1985.

[132] M. S. Hunter, B. Segelke, M. Messerschmidt, G. J. Williams, N. A. Zatsepin, A. Barty, W. H. Benner, D. B. Carlson, M. Coleman, A. Graf, S. P. Hau-Riege, T. Pardini, M. M. Seibert, J. Evans, S. Boutet, and M. Frank, "Fixed-target protein serial microcrystallography with an x-ray free electron laser," *Scientific Reports*, vol. 4, 2014.

[133] C. R. D. Lancaster, "Ubiquinone reduction and protonation in photosynthetic reaction centres from *Rhodopseudomonas viridis*: X-ray structures and their functional implications," *Biochimica et Biophysica Acta - Bioenergetics*, vol. 1365, no. 1-2, pp. 143–150, 1998.

[134] J. Koepke, E. M. Krammer, A. R. Klingen, P. Sebban, G. M. Ullmann, and G. Fritzsch, "pH modulates the quinone position in the photosynthetic reaction center from *Rhodobacter sphaeroides* in the neutral and charge separated states," *Journal of Molecular Biology*, vol. 371, no. 2, pp. 396–409, 2007.

[135] T. Weinert, N. Olieric, R. Cheng, S. Brünle, D. James, D. Ozerov, D. Gashi, L. Vera, M. Marsh, K. Jaeger, F. Dworkowski, E. Panepucci, S. Basu, P. Skopintsev, A. S. Doré, T. Geng, R. M. Cooke, M. N. Liang, A. E. Prota, V. Panneels, P. Nogly, U. Ermler, G. Schertler, M. Hennig, M. O. Steinmetz, M. T. Wang, and J. Standfuss, "Serial millisecond crystallography for routine room-temperature structure determination at synchrotrons," *Nature Communications*, vol. 8, 2017.

[136] M. Caffrey, "Membrane protein crystallization," *Journal of Structural Biology*, vol. 142, no. 1, pp. 108–132, 2003.

[137] S. A. Kolek, B. Bräuning, and P. D. S. Stewart, "A novel microseeding method for the crystallization of membrane proteins in lipidic cubic phase," *Acta Crystallographica Section F: Structural Biology Communications*, vol. 72, pp. 307–312, 2016.

[138] O. Shlyk, I. Samish, M. Matěnová, A. Dulebo, H. Poláková, D. Kaftan, and A. Scherz, "A single residue controls electron transfer gating in photosynthetic reaction centers," *Scientific Reports*, vol. 7, 2017.